Wageningen University

Meteorology and Air Quality Group

MSc thesis

Quantifying NO_x emissions from Paris with high-resolution satellite measurements

Author
M.B. (Maarten) de Zeeuw

Supervisor
Dr. K.F. (Folkert) Boersma

Examiner
Prof. Dr. M.C. (Maarten) Krol

February 13, 2019

Abstract

The new high-resolution TROPOMI satellite observations make it now possible to measure nitrogen dioxide (NO_2) at city level from space. Especially in cities nitrogen dioxides (NO_x) pose a threat to air quality, since large numbers of people and strong emission sources are concentrated together. This study evaluated and developed a simple column model approach to quantify these NO_x emissions for Paris from day-to-day with the first TROPOMI observations. The influence of downwind emissions, diurnal variation in emissions, lifetime variability, and background decay on the column model's simulated downwind decay were examined. Because these influences on the downwind plume showed to change the estimated NO_x lifetime by up to a factor of 3, the NO_x emission was estimated just from the increase in NO_2 in the wind direction over Paris as measured by TROPOMI. The resulting average estimated NO_x emission from Paris of eleven days (in November 2017, February and April 2018) was 55.9 mol s^{-1} during weekdays and 30.2 mol s^{-1} during weekends, which is respectively 24% and 51% smaller than the EDGAR emission inventory from 2012. This research demonstrated how TROPOMI's high-resolution observations can be used to estimate NO_x for single days. Such an approach can be a fast and understandable tool for evaluating the effectiveness of air quality and climate mitigation measures.

Acknowledgements

This thesis would not have been possible without Folkert Boersma's supervision. Not only was his guidance and constructive feedback very important for this work, his enthusiasm and our fruitful discussions also inspired me to continue further. Also working together with Alba Lorente in the same direction was a good way to ensure that my results were correct and useful. All other MSc students in the MAQ thesis ring helped to improve my writing. Besides, I also acknowledge the Royal Netherlands Meteorological Institute (KNMI) for providing the very first TROPOMI NO_2 observations, as well as the European Commission's Joint Research Centre for the EDGAR inventory, Météo-France and the University of Wyoming for the radiosondes at Trappes and Airparif for the surface NO_2 measurements.

Contents

Abstract i

Acknowledgements ii

Contents iii

1 Introduction 1

2 Background 2
2.1 Tropospheric nitrogen dioxides . . . 2
2.2 Emission monitoring . . . 2

3 Data description 4
3.1 TROPOMI observations . . . 4
3.2 EDGAR emission inventory . . . 5
3.3 Radiosondes in Trappes . . . 6
3.4 Paris surface observations . . . 6
3.5 Day selection criteria . . . 6
3.6 First validation of TROPOMI over Paris . . . 7

4 Applying the column model 9
4.1 Methodology . . . 9
4.1.1 Line density . . . 9
4.1.2 Column model to simulate line densities . . . 11
4.1.3 Estimating emissions with the column model . . . 12
4.2 Results . . . 13
4.3 Discussion . . . 14
4.3.1 Quantifying NO_x emissions from Paris . . . 14
4.3.2 Estimating the NO_x lifetime . . . 15

5 Influences on downwind decay 16
5.1 Methodology . . . 16
5.1.1 Downwind emissions . . . 16
5.1.2 Diurnal emissions . . . 18
5.1.3 Variability in lifetime . . . 19
5.1.4 Background decay . . . 20
5.2 Results . . . 21
5.3 Discussion . . . 23

6 Accumulation over the source area 24
6.1 Methodology . . . 24
6.1.1 Comparison with surface observations . . . 24
6.1.2 Estimating emission from source area accumulation . . . 24
6.1.3 Spatial column model for emission pattern over the source area . . . 25
6.2 Results . . . 26

6.3 Discussion 31

7 Conclusion **33**

References **35**

1 Introduction

Atmospheric nitrogen oxides ($NO_x = NO + NO_2$) have an adverse effect on public health and also influence the climate. This is especially an important issue in cities, where both large numbers of people and strong NO_x emissions from traffic, heating and industry are concentrated. In Paris, for instance, around 1.3 million inhabitants were exposed to an annual mean nitrogen dioxide (NO_2) concentration that exceeded the EU limit of 40 μg m^{-3} in 2017 (Airparif, 2018). To comply with the EU air quality norms by 2025, the city of Paris is currently planning 46 new mitigation measures in their latest atmospheric protection plan (DRIEE, 2018). These measures range from stimulating cycling to imposing more stringent emission norms on industry, but also include additional actions during strong pollution episodes.

Such air quality and climate mitigation plans require monitoring of NO_x emissions to evaluate their effectiveness. This emission monitoring is often done with a bottom-up approach, where the emission is calculated based on activity data and corresponding emission factors. However, there are substantial uncertainties in this method (Crippa et al., 2018; Kuenen et al., 2014), for instance because the exact location of emission is not known. That is why these bottom-up emission inventories are validated with measurements, the so-called top-down approach, often in combination with a model that relates observed atmospheric concentrations to emissions. Such a top-down study based on MAX-DOAS observations by Shaiganfar et al. (2017) found between 1.4 and 2.3 times higher NO_x emissions from Paris compared to bottom-up emission inventories.

Also top-down studies that use satellite observations of NO_2 have resulted in important insights into NO_x emission sources. Because the spectrometers on these satellites measure reflected solar radiation from which tropospheric NO_2 columns are retrieved, they grasp all the NO_x that has been emitted. For example, Akimoto et al. (2006) showed that the coal consumption of China was significantly under reported from 1996 to 2003. In addition, temporally averaged remote sensing observations of NO_2 have been used to quantify emissions of isolated sources such as ship tracks (Vinken et al., 2014) and megacities (Beirle et al., 2011).

On 13 October 2017, a new satellite with the TROPOspheric Monitoring Instrument (TROPOMI) was launched, a spectrometer that allows observation of key atmospheric compounds, including NO_2 (Veefkind et al., 2012). This new instrument provides daily global measurements at a resolution of 3.5×7 km^2, which is more than three times finer than its predecessor OMI. With approximately 130 pixels over Paris, TROPOMI makes it possible to examine tropospheric NO_2 columns at city level. This raises the question how these new high-resolution NO_2 column observations can allow a better quantification of NO_x emissions.

This study aims to evaluate and develop a simple column model approach to quantify the NO_x emissions of Paris from single-day TROPOMI observations. The column model, as explained by Jacob (1999), describes the chemical evolution of a pollutant in the wind direction as a function of the emission, chemical decay and wind speed. The emission estimates from the column model are compared to the bottom-up EDGAR emission inventory. In chapter 4, this method is introduced for 22 November 2017, one of the first TROPOMI observations at cloud-free conditions over Paris, showing a distinct NO_2 plume. Different factors that influence the decay downwind of Paris are further evaluated in chapter 5. Since these downwind influences on the column model estimates of the NO_x lifetime were shown to be large, the last part of this study, chapter 6, estimates NO_x emissions just from the increase in NO_2 along the wind direction over the source area. This is done for ten selected days in the months February to April 2018 and optimally shows the new possibilities of TROPOMI's higher resolution

2 Background

2.1 Tropospheric nitrogen dioxides

According to the World Health Organization, exposure to NO_2 is linked to a reduced long function and increased bronchitis symptoms of asthmatic children (WHO, 2016). Also the ozone (O_3) that is formed from NO_2 has a negative effect on human health; it can cause breathing problems and lung diseases and is associated with increasing mortality rates. Besides health impacts, O_3 and hydroxyl (OH) radicals formed from tropospheric NO_2 also have an impact on climate: the former acts as a greenhouse gas and the latter enhances the oxidation and shortens the lifetime of methane (CH_4), the second most significant anthropogenic greenhouse gas. Finally, the deposition of HNO_3 causes fertilisation of soils and surface waters.

Although almost all NO_x is emitted as nitrogen oxide (NO), there is a rapid cycling between NO and NO_2 in the atmosphere (Jacob, 1999). NO reacts with O_3 to form NO_2 and the reverse reactions is possible in the presence of oxygen and solar radiation. Fossil fuel combustion accounts for about half of the NO_x present in the troposphere, while biomass burning, mainly from tropical agriculture and deforestation, comprises another quarter (Jacob, 1999, p. 212).

In the troposphere, NO_x has a short lifetime, in the order of one day, mainly because of the oxidation of NO_2 to HNO_3 after which HNO_3 is scavenged by precipitation. During daytime NO_2 is oxidised by OH, whereas at night HNO_3 is formed through NO_3 and N_2O_5. A smaller sink is the oxidation of NO_2 to peroxyacetylnitrate (PAN), which is enabled by the presence of photo-chemically oxidised hydrocarbons. The lifetime of PAN is strongly dependent on temperature, so that PAN that is present in the middle and upper troposphere can be transported over long distances before it decomposes back to NO_x.

Tropospheric NO_x also has an important role in the cycle of OH. The photo-chemical processing of NO_2 results in the production of NO and O_3, which can photolyse and produce OH molecules that enable the oxidation of CO and CH_4.

2.2 Emission monitoring

Bottom-up emission inventories, based on activity data and corresponding emission factors, have large uncertainties in the reported NO_x emissions. In the TNO-MACC emission inventory, the uncertainty ranges from 20% up to 300% for different source categories (Kuenen et al., 2014). In the Atmospheric Database for Global Atmospheric Research (EDGAR) v4.3.2 inventory of 2012, which is used in this research, the uncertainty in NO_x emission from different regions varies from 17.2% to 69.4% (Crippa et al., 2018). And specifically for megacities, Butler et al. (2008) found that three different emission inventories often differ by a factor of two for the same city, which could possibly be explained by the fact that the spatial allocation of emissions is based on population density rather than the actual point of emission.

Top-down studies on NO_x emissions based on satellite measurements have been an important tool to evaluate bottom-up accounting. This satellite monitoring of NO_x emissions can be distinguished in three different approaches:

1. Formal inversions using chemistry transport models (e.g. Martin et al., 2003)
2. Comparisons between the change in reported NO_x emissions and observed NO_2 columns (e.g. Jiang et al., 2018)

3. A column model for single source areas (e.g. Beirle et al., 2011)

Although the total global NO_x emission estimated with the top-down approach based on satellite observations in combination with atmospheric models generally align closely with bottom-up reported global annual emissions (e.g. Martin et al., 2003), these top-down studies often indicate large discrepancies in the magnitude, temporal variation and regional distribution of emission sources compared to bottom-up inventories. In the United States, NO_2 satellite measurements of OMI show a slower reduction than the predicted NO_x emission trend of the Environmental Protection Agency's inventory from 2011 to 2015 (Jiang et al., 2018). Martin et al. compared emissions derived from GOME and an inverse model with the GEIA and EDGAR 3.0 emission inventory and found significant regional differences (2013). Richter et al. found a stronger positive trend in the tropospheric NO_2 concentration over China in satellite observations than bottom-up inventories (2005). Another study on NO_x emissions in China that used the different passing time of GOME-2A and OMI found clear local differences (Lin et al., 2010). Finally, satellite observations also enable studies on the weekly or seasonal cycle of NO_2 (e.g. Beirle et al., 2003). These local and temporal differences can have an important influence on the accuracy of modelling studies that use bottom-up emission inventories, especially because of the short lifetime of NO_x.

Besides top-down studies at global or continental scales, temporally averaged satellite observations have been used to directly estimate emissions from a single emission source. Vinken et al. found that shipping emissions are both overestimated (up to 60%) and underestimated (up to 131%) in comparison to the EMEP inventory (2014). Another example is a study by Wang et al., which used OMI observations and a global chemical transport model to investigated the contribution of new coal power plants in China to NO_x emissions (2012).

Rather than using a full chemical transport model, NO_x emissions from a single source area have also been successfully estimated with a column model similar to the method described in Jacob (1999). De Foy et al. evaluated different implementation of this approach to estimate surface emissions and lifetimes from satellite measurements (2014). Beirle et al. has applied this method successfully to estimated NO_x emissions and lifetimes from ship tracks (2004), as well as from megacities (2011). This showed generally a good agreement with the EDGAR inventory, but an underestimation of 300% for the city of Riyadh.

However, these column model studies require averaged data for multiple years to enhance the spatial resolution. That is why the advancement in resolution of TROPOMI (described in chapter 3) is particularly promising for estimating NO_x emissions with this third satellite emission monitoring approach. This could enable a quantification of daily emissions rather than annual averages based on a single TROPOMI orbit.

3 Data description

3.1 TROPOMI observations

Currently, four satellites are orbiting the planet to monitor tropospheric NO_2: GOME-2A, GOME-2B, OMI and its successor TROPOMI (Boersma et al., 2018). The GOME-2 instrument passes the equator at 10:30 local time, while the OMI and TROPOMI both have an early afternoon overpass of respectively 13:40 and 13.30 local time (Boersma et al., 2018; Veefkind et al., 2012). The precise TROPOMI overpass times at Paris for the selected days are listed in Table 3.1.

The tropospheric NO_2 column is retrieved from the spectrometer measurements of direct and backscattered solar radiation with an algorithm, such as DOMINO v2.0 (Boersma et al., 2011) and SP2 (Buscela et al., 2013) for OMI. An update of the DOMINO v2.0, the new QA4ECV product, is now available for the OMI and GOME-2A observations, which started respectively in 2004 and 2007, as well as for past measurements by GOME-2A, from 1996 to 2003, and SCIAMACHY, from 2000 to 2012 (Boersma et al., 2018). For TROPOMI, a retrieval algorithm similar to QA4ECV is used (van Geffen et al., 2016). The general functioning of this retrieval procedure can be described in three steps (ibid.):

1. Derive the NO_2 slant columns from the measured radiance and irradiance spectra with the Differential Optical Absorption Spectroscopy (DOAS) method.
2. Separate the tropospheric and stratospheric component of the slant columns.
3. Convert the tropospheric and stratospheric slant columns to a vertical column based on the tropospheric air mass factor (AMF).

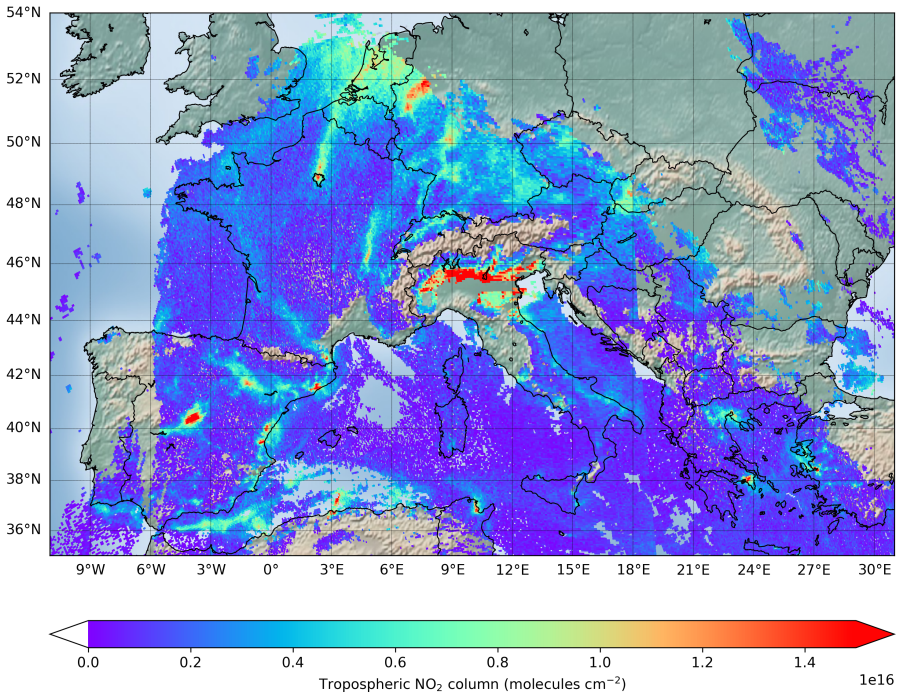

Figure 3.1: Tropospheric NO_2 columns observed by TROPOMI on 22 November 2017 over Europe with AMF, albedo and cloud fraction filters.

The NO_2 tropospheric column is observed with a spatial resolution of 3.5×7 km^2, much higher than OMI's resolution of 13×24 km^2 (Boersma et al., 2011). In comparison to its predecessor OMI, the new TROPOMI spectrometer (described by Veefkind et al., 2012) has an extended wavelength range with bands in the NIR and SWIR in addition to the UV and VIS range. This new NIR band provides information about cloud characterisation and enables a better cloud correction, resulting in a smaller error for partly cloudy conditions. In addition, it is expected that the smaller pixel size of TROPOMI observations leads to 70% more cloud-free retrievals in comparison to OMI, since even a small clouds affects the whole pixel (Krijger et al., 2007). Furthermore, TROPOMI's signal-to-noise ratio is a factor 2-3 higher than OMI.

In chapter 4 of this study, preliminary TROPOMI data of 22 November 2017 is used, with cloud free conditions over central Europe, showing the tropospheric NO_2 columns and a distinct north-northeasterly plume originating from Paris (Figure 3.1). For the last section, chapter 6, TROPOMI observations of two periods were analysed: 22 to 26 February 2018 and 17 to 24 April 2018. This preliminary data is from the commissioning phase and hence a good test of the usefulness of the early-mission data quality before the public data release on 11 July 2018. TROPOMI data is now available via the Copernicus Open Access Hub[1].

3.2 EDGAR emission inventory

To compare the emissions that are derived from the TROPOMI observations, the bottom up emission inventory EDGAR v4.3.2[2] of 2012 is used as reference (Figure 3.2). This version of the EDGAR emission inventory is described by Crippa et al. (2018). The EDGAR emissions in EU28 countries, which includes Paris, are reported to have an uncertainty of 50.7% (ibid.). These reported emissions are based on activity data and spatial distribution proxies from Janssens-Maenhout et al. (2017), similar to the EDGAR greenhouse gas emission inventory, and emission factors from the EEA Guidebook (2013), HTAP_v2 (Janssens-Maenhout et al., 2015) and PEGASOS (Crippa et al., 2016).

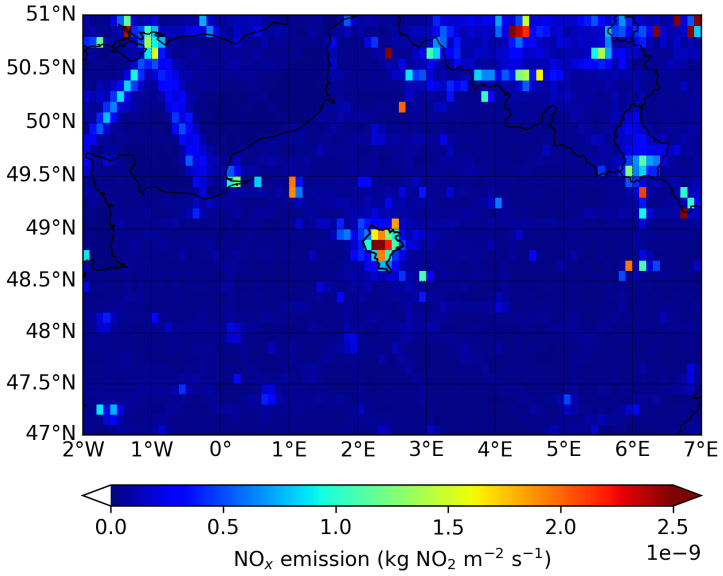

Figure 3.2: NO_x emissions, expressed in NO_2, from the EDGAR inventory from 2012 for Paris and its surroundings.

[1] https://scihub.copernicus.eu/
[2] https://data.europa.eu/doi/10.2904/JRC_DATASET_EDGAR

3.3 Radiosondes in Trappes

Every day at noon a sounding is performed by Meteo France at Trappes, approximately 30 km West-Southwest of the centre of Paris, which gives the vertical profile of, among other variables, the wind speed and direction (Table 3.1). The boundary layer height is determined from the inversion in the potential temperature profile (Table 3.1). These radiosonde observations are available via the University of Wyoming[3] and the surface observations via the National Oceanic and Atmospheric Administration[4]. It should be noted that the site is located 168m above sea level, whereas the centre of Paris is approximately 130 meters lower.

3.4 Paris surface observations

Surface NO and NO_2 observations in the Paris area are available from Airparif[5]. Air is analysed using catalytic reduction and chemiluminescence according to the European EN 14211 standard (Jordan Bureau, personal communication, 24 August 2018). The hourly averages for 40 observations sites that measure NO_2 concentrations in μg m^{-3} were available, of which 13 traffic stations were excluded because of strong local contributions from traffic and 4 outside the domain of the source area. The location of the stations is shown in the maps in Figure 6.2 and 6.3. In addition, NO and NO_2 concentrations are measured at the top of the Eiffel Tower at a height of 315 m, which gives important information on the vertical distribution and is more representative for the whole city rather than surface stations that measure concentrations influenced by emissions at street level.

3.5 Day selection criteria

Not all days have TROPOMI observations that are suited to estimate emissions with the column model approach. The main limitation is that only days which are largely cloud fee can be used, since clouds screen the lowest part of the atmosphere where NO_x emission takes place. Overall, three conditions were considered for the day selection in this study:

1. Cloud-free conditions are required to interpret the increase and decay of NO_2 along with the wind.
2. No problems in the tropospheric AMF, which is tested by dividing the difference between the slant column density and the stratospheric slant column density by the geometric AMF.
3. A sufficiently strong wind speed so that an increase in NO_2 over the source area in the wind direction can be observed, from which the NO_x emission can be determined with the column model.

Chapter 4 uses TROPOMI observations from 22 November 2017, as this was one of the first available days showing a clear plume from Paris (Figure 3.3a). From the period February to April 2018, two sequences of days were cloud free: 22 to 26 February and 17 to 24 April. The orbit of 24 February 2018 was excluded because of problems in the tropospheric AMF. Two more days in April 2018 were excluded: the 20th because of strong stagnant and partly cloudy conditions shown by little outflow of NO_2 out of the source area (Figure 3.3b) and the 23rd because of a high cloud fraction over Paris. This results in a total of eleven days that are used.

[3] http://weather.uwyo.edu/upperair/bufrraob.shtml
[4] https://www.ncdc.noaa.gov/isd
[5] https://www.Airparif.asso.fr/stations

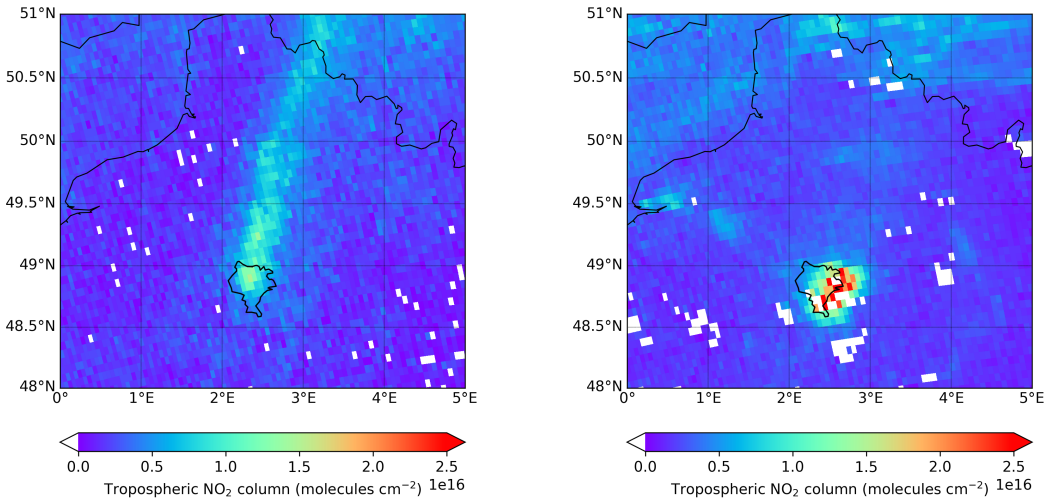

(a) 22 November 2017

(b) 20 April 2018

Figure 3.3: Tropospheric NO_2 columns observed by TROPOMI over Paris (denoted by the black outline) and its surrounding region with AMF, albedo and cloud fraction filters.

3.6 First validation of TROPOMI over Paris

In principle, one could calculate an NO_2 column by integration the concentration measured at the Eiffel Tower up to the boundary layer height, assuming that the boundary layer is well-mixed and that the NO_2 concentration is constant with height. However, the results of this approach deviate substantially with the tropospheric NO_2 columns measured with TROPOMI (Table 3.1). Only for three days out of ten days the Eiffel Tower column and TROPOMI column differ by less then 25%. Except for 22 November 2017, all the Eiffel Tower columns are substantially higher. The Eiffel Tower column is even a factor 5 higher than the TROPOMI tropospheric column on 24 February 2018, a day with a relatively high boundary layer height of 2000 m.

The higher Eiffel Tower column suggests that NO_2 is not fully mixed within the boundary layer and that the concentration is higher at the surface. This is also shown by NO_2 measurements with a ground-based UV-visible light spectrometer in the centre of Paris (Dieudonné et al., 2013). Such a vertical NO_2 gradient is also expected, since NO_2 is continuously emitted at the surface. Thus assuming that the Eiffel Tower measurements are representative for the full boundary layer leads to an overestimation of the column.

Table 3.1: Overview of all selected days, with TROPOMI overpass time at Paris, boundary layer height (h), as well as wind speed (U) and direction in the middle of the boundary layer from sounding observations at Trappes. Surface wind speed and direction at Trappes are also given. Wind data marked with an asterisk is the boundary layer mean from the ECMWF-Interim reanalysis (unpublished paper, Lorente et al., 2018). TROPOMI tropospheric NO_2 column are given in comparison to the calculated NO_2 column based on Eiffel Tower measurements and h.

			Boundary layer			Surface		Column	
Date	Day	Overpass (UTC)	h (m)	U (m s^{-1})	Direction (degrees)	U (m s^{-1})	Direction (degrees)	TROPOMI ($\cdot 10^{16}$ NO_2 molecules cm^{-2})	Eiffel Tower
22/11/17	Wednesday	12:52	500	8.8	185	4.6	190	1.5	1.2
22/02/18	Thursday	12:26	874*	8.6*	50*	5.7	50	1.2	3.1
23/02/18	Friday	12:07	907*	9.0*	60*	7.2	60	0.9	2.4
24/02/18	Saturday	13:30	2000	5.7	26	7.2	50	0.9	4.7
25/02/18	Sunday	13:11	1000	9.3	54	6.7	40	0.7	1.3
26/02/18	Monday	12:52	1400	9.8	50	8.2	60	0.9	2.2
17/04/18	Tuesday	12:12	1250	5.7	186	3.6	200	0.8	1.0
18/04/18	Wednesday	11:53	1350	8.2	99	5.1	120	0.9	3.2
19/04/18	Thursday	13:16	750	4.1	194	4.1	220	0.9	1.1
20/04/18	Friday	12:57	1700	4.6	289	3.1	10	1.1	4.2
21/04/18	Saturday	12:38	1500	4.1	83	3.1	150	1.1	2.7
22/04/18	Sunday	12:19	2188*	9.7*	230*	4.6	230	0.4	1.1
24/04/18	Tuesday	13:23	1200	4.6	209	4.1	220	0.2	-

4 Applying the column model

The TROPOMI observations from 22 November 2017, illustrated in Figure 3.3a, show accumulation of NO_2 over Paris along with the wind followed by a decaying plume downwind of the source area. From these measurements, a one-dimensional line density is calculated in this chapter, which gives the evaluation of the number of NO_2 molecules at a certain distance from the source area along the wind direction. Subsequently, the NO_x emission rate can be estimated with a column model similar to Jacob (1999) from this line density and minimal additional model input. This study focuses on the city of Paris, as it has a substantial source area, only limited emission sources in its surrounding, and one of the first TROPOMI observations shows a distinct plume from Paris on 22 November 2017.

4.1 Methodology

4.1.1 Line density

The tropospheric NO_2 columns from the TROPOMI observations are selected as a function of the distance from the source area of Paris in the wind direction (x) and integrated perpendicular to the wind direction (y), similar to the approach used by Beirle et al. (2011). This line density represents the change in the NO_2 column along with the wind, showing a steep increase in NO_2 as the column moves over Paris and a slower decay as the column moves away from the source area. The wind direction in the middle of the boundary layer is selected from the radiosonde measurements at Trappes.

The line density starts 30 km from the centre of Paris and continues in the direction from the wind, see Figure 4.1. The source area runs from 0 to 60 km on the line density, which represents approximately the greater Paris area (Métropole du Grand Paris). The line density continues up to 140 km downwind of the source area. Although it appears from the TROPOMI observation that the plume is still visible more than 140 km downwind on 22 November 2017, this boundary is chosen to avoid mixing up the plume from Paris with local enhancements in NO_2 from fresh emissions, since the EDGAR emission inventory shows some relatively large emission sources further downwind close to the French-Belgium border (Figure 3.2).

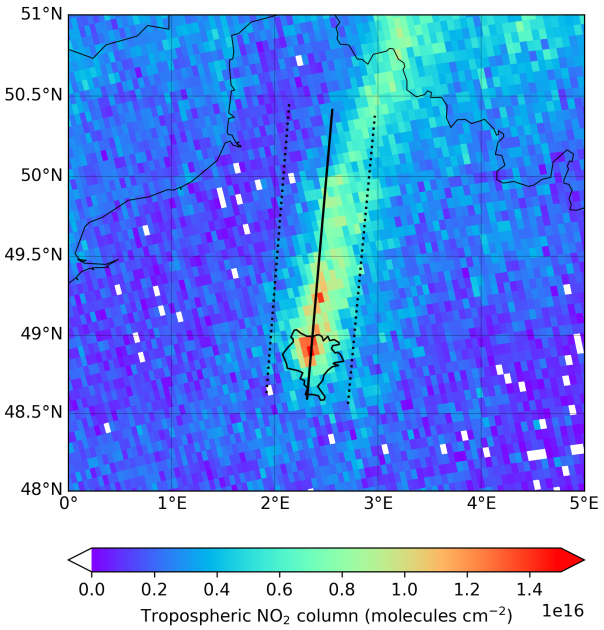

Figure 4.1: Tropospheric NO_2 columns observed by TROPOMI on 22 November 2017. The greater Paris region, integration line and across track integration boundaries are delineated by the black lines. For the white pixels, the measurements have been excluded based on the AMF, albedo and cloud fraction criterion.

For every interval of 3.5 km (similar to TROPOMI's resolution) on the line that passes through the centre of Paris (48°51'53.0"N 2°20'56.5"E) in the wind direction, the tropospheric NO_2 column (N_{NO_2}) pixels at a location (x, y) that are perpendicular to and within a distance of 30 km from the centre line ($y = 0$) are selected. Both the centre line in the x direction and the perpendicular lines in the y direction are illustrated in Figure 4.2. The total source area is hence 60 by 60 km^2, tilted in the direction of the wind and with the centre of Paris in the middle. The selected columns are multiplied by the intersection length (δy) of the borders of the pixel with the line perpendicular to the wind direction to obtain the line density for each selected pixel (Figure 4.2, where the $\times$ markers denote the intersections). This intersection length can vary from very small up to the length of the diagonal of the pixel (7.8 km). The selected pixel line densities ($N_{NO_2}(x, y) \cdot \delta y$) are subsequently summed, resulting in the total line density in NO_2 molecules cm^{-1} at x:

$$L_{NO_2}(x) = \sum_{-30<y<30} N_{NO_2}(x, y) \cdot \delta y \tag{4.1}$$

Measurements with a tropospheric air mass factor (AMF) lower than 0.2, surface albedo higher than 0.3 and cloud radiance fraction in the NO_2 window higher than 0.5 are excluded. These excluded pixels are replaced with the average of the line density at this distance, for instance for the pixel in the lower left corner in Figure 4.2. If half of the across length does not meet these selection criteria, then no line density is given for that interval since the line density would not be representative for entire domain length.

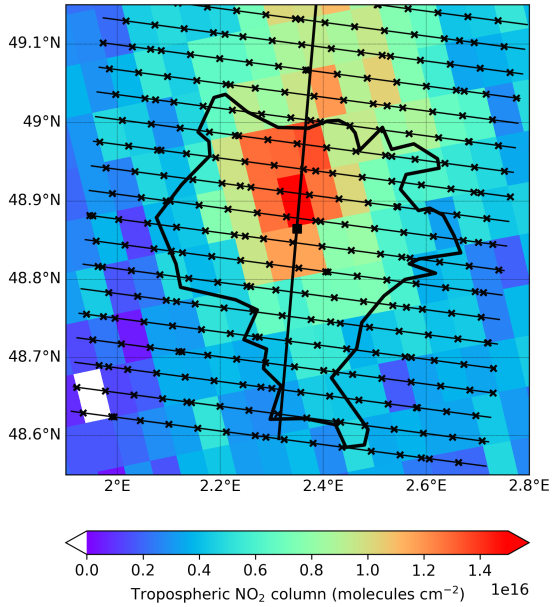

Figure 4.2: Line density derivation and tropospheric NO_2 columns over the greater Paris region on 22 November 2017. The centre line starts 30 km from the centre of Paris (denoted by the square) and proceeds in the direction of the wind (x). For each of the lines at distance x perpendicular to the wind direction (y) a line density is calculated, which is the sum of all the pixels on this line multiplied by the intersection length of the respective pixel with this line (δy). The intersection length is illustrated as the distance between the $\times$ markers in this figure.

4.1.2 Column model to simulate line densities

The column model, described in Jacob (1999), simulates the chemical evolution of a pollutant in a well-mixed column of air moving in the direction of the wind with speed U, passing a source area with length x_s with a constant emission rate E of NO_x in molecules cm^{-1} s^{-1}. Here the column has the width of the plume of 60 km as defined in the line density derivation. Since most of the tropospheric NO_2 is present in the boundary layer, the height of the modelled column represents this layer. The wind speed for the middle of the boundary layer is derived from the sounding observations at Trappes. The background line density is represented by the constant B.

A first-order chemical loss is assumed with a rate constant k of NO_x, which is inversely proportional to the effective lifetime of NO_x (τ_{NO_x}) in the plume. During the middle of the day, this loss is primarily determined by the reaction of NO_2 with OH to HNO_3 (Seinfeld and Pandis, 2006):

$$NO_2 + OH + M \xrightarrow{k_2} HNO_3 + M \tag{R4.2}$$

The NO_x lifetime in hours can be calculated as a function of the rate constant of reaction R4.2, the OH concentration and the NO_x/NO_2 ratio:

$$\tau_{NO_x} = \frac{1}{k} = \frac{1}{k_2[OH]} \cdot \frac{[NO_x]}{[NO_2]} \tag{4.3}$$

The line density of NO_x at distance x along the wind direction is then given by the following two formulas:

$$L_{NO_x}(x) = \frac{E}{k}\left(1 - e^{-\frac{kx}{U}}\right) + B \text{ for } 0 \leq x \leq x_s \tag{4.4}$$

$$L_{NO_x}(x) = L_{NO_x}(x_s)e^{-\frac{k(x-x_s)}{U}} + B \text{ for } x > x_s \tag{4.5}$$

Equation 4.4 describes the accumulation of NO_x as the column passes the source area with length x_s in the main wind direction. The first term on the right-hand side of this equation denotes the NO_x emission strength over the full width of the column (60 km) proportional to the rate constant. The second term on the right-hand side of equation 4.4 describes the exponential chemical decay (reaction 4.2) as a function of x, which becomes the only factor once the column moves away from the emission source as described in equation 4.5. Thus the steepness of the decay in the line density together with the average wind speed is a measure for the chemical conversion that determines the NO_x lifetime. This model assumes a constant background, a uniform wind speed with height and in time, zero downwind emissions and no temporal variability in the emission and loss rate of NO_x.

4.1.3 Estimating emissions with the column model

The column model can not only be used to simulate a line density, but also to estimate emissions as well as the lifetime and background line density. Yet it is important to first account for the difference in units when converting from line density to emission: TROPOMI measures the number of NO_2 molecules, while the emission describes the amount of NO_x. Here an average correction factor is applied for the NO_x/NO_2 ratio of 1.32, a typical value for urban conditions around noon, similar to Beirle et al. (2011) based on Seinfeld and Pandis (2006):

$$\frac{[NO_x]}{[NO_2]} = \frac{L_{NO_x}}{L_{NO_2}} = \frac{\tau_{NO_x}}{\tau_{NO_2}} \approx 1.32 \tag{4.6}$$

This average value is compared to the ratio of the NO_x and NO_2 mixing ratios as observed at the 300 m level of the Eiffel Tower. If the boundary layer is well-mixed, then these measurements are representative for the whole layer, whereas surface observations would be perturbed by nearby emissions.

To obtain top-down estimates of E, k and B, equation 4.4 and 4.5 are simultaneously fitted to the TROPOMI line density based on a non-linear least squares regression. This approach assumes that E is constant in time and over the city and that τ_{NO_x} can be estimated with a single time-independent value. For a wide range of values of E, k and B, numerous line densities are simulated (L_m) from which the residuals with n TROPOMI line densities (L_o) over the standard error of the TROPOMI line density (σ) are calculated with the Levenberg-Marquardt algorithm. The optimal parameters and corresponding covariances from which the standard deviation is derived are selected from the simulated line density that results in the lowest chi squared (χ^2):

$$\chi^2 = \sum_{i=1}^{n}\left(\frac{L_o(x_i) - L_m(x_i, E, k, B)}{\sigma(x_i)}\right)^2 \tag{4.7}$$

The standard error of each line density at x_i is given by equation 4.8, which accounts for the different relative contributions of each pixel $N(x_i, y)$ with intersection length δy to the total line density $L(x_i)$ with length Δy (60 km):

$$\sigma(x_i) = \sqrt{\sum_{-30<y<30}\left(\frac{\delta y(x_i, y)}{\Delta y} \cdot \left(N(x_i, y) - \frac{L(x_i)}{\Delta y}\right)\right)^2} \tag{4.8}$$

In order to compare the resulting top-down emission estimate from the TROPOMI line density, the EDGAR NO_x emissions in kg s^{-1} are expressed as NO_2 and therefore converted to mol s^{-1} with the molecular weight of NO_2.

4.2 Results

The line density from the TROPOMI observations on 22 November 2017 shows a steep increase in NO_2 over Paris (x < 60 km), while the amount of NO_2 decreases slower downwind of the source area due to chemical decay (Figure 4.2). Subsequently, the emission, lifetime and background concentration is estimated by fitting the column model (Function 4.4 and 4.5) to this line density. The simulated line density leading to the best match with the observed line density has a NO_x emission of 74.6 ± 4.58 mol s^{-1}, lifetime of 3.7 ± 0.28 hours and background of 1.6 ± 0.09 $\cdot 10^{22}$ molecules cm^{-1} (Table 4.1). This emission estimate from the TROPOMI line density on 22 November 2017 is 38% higher than the EDGAR NO_x emission inventory from 2012, which gives a value of 54.1 mol s^{-1} for the same source domain. The non-linear least squares fit has an R^2 value of 0.55 compared to the TROPOMI line density.

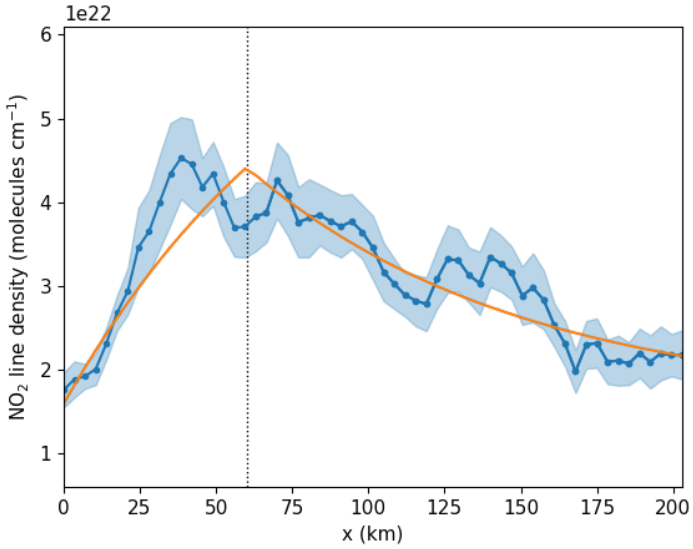

Figure 4.3: NO_2 line density from the TROPOMI observations on 22 November 2017 (blue) and the line density from the inverse column model (orange). The dotted line indicates the length of the source area and the shaded area shows the standard error of the line densities.

Table 4.1: Estimates of the NO_x emission, lifetime and NO_2 background line density and their standard deviations from fitting the column model to the TROPOMI line density of 22 November 2017.

Parameter	Estimate	Standard deviation	Unit
Emission	74.6	4.68	mol s^{-1}
Lifetime	3.7	0.28	hours
Background	1.6	0.09	$\cdot 10^{22}$ molecules cm^{-1}

This R^2 value indicates that the column model can replicate 55% of the variability in the observed TROPOMI line density. It is clear from Figure 4.3 that neither the increase over the source area nor the downwind decrease follow the exponential functions from the column model

completely. The TROPOMI line density shows the steepest increase at x=25 km, in the middle of the source area. Hence the TROPOMI line density is lower than the simulated line density over the first part of the source area, then becomes higher until it peaks at x=40 km and finally drops again below the observed line density for the last 10 km of the source area, suggesting that emissions are not constant over the city. This fluctuation in the TROPOMI line density is also present in the downwind decay part of the plume and not reproduced by the column model.

The emission estimate for 22 November 2017 from the TROPOMI line density is based on the average NO_x/NO_2 ratio of 1.32. However, the observations at the Eiffel Tower at 13.00 UTC give a ratio of 1.72, which would result in a 30% higher emission (99.3 mol s^{-1}).

4.3 Discussion

4.3.1 Quantifying NO_x emissions from Paris

The NO_x emission estimate from the TROPOMI line density from 22 November 2017 is 38% higher than the average EDGAR emission of 54.1 mol s^{-1} over the same area. However, it should be noted that these two emission numbers require a different interpretation. On the one hand, the emission estimate from the TROPOMI observations represents the emissions during the hours before the time of the measurement around noon. So for 22 November 2017, this would approximately be the period from 11:00 to 12:52 (x_s/U = 1.9 hours). The EDGAR emissions, on the other hand, are an annual average, even though they are not constant over time in reality. Van der Gon et al. (2006) provides generalised temporal emission profiles for European air quality modelling, showing that NO_x emissions are above the average during winter, on weekdays and during daytime. Based on these temporal factors, the emission on a weekday in November between 12.00 and 13.00 hour is 30% higher then the annual average, where this variability is 5% monthly, 6% weekly and 19% diurnal. Hence the top-down emission estimate of 74.6 mol s^{-1} from the TROPOMI observations would be slightly higher than the emission from Paris in the EDGAR inventory, which would be 70.3 mol s^{-1}, when accounting for temporal variability. When temporal variability is considered, the TROPOMI NO_x estimate is hence consistent with EDGAR within 10%.

Yet the TROPOMI emission estimate might also be too low, since the NO_x/NO_2 ratio as observed at the Eiffel Tower is higher than the average ratio that was applied. When the Eiffel Tower NO_x/NO_2 ratio is used (1.72 instead of 1.32), the top-down emission and lifetime estimate would also be 30% higher (97.3 mol s^{-1} and 4.9 hours). A study by Shaiganfar et al. (2017) with the CHIMERE model also found higher ratios during winter (1.51) than during summer (1.32) for the Paris region, which can be explained by higher ozone mixing ratios in summer. In addition, they found that the daily values could deviate by up to 30% from the seasonal mean. Thus, this top-down emission monitoring approach might require a more refined NO_x/NO_2 rationing method. This ratio could for instance be obtained from tall-tower observations such as the Eiffel Tower or an atmospheric chemistry model, although the accuracy of such methods needs to be evaluated.

The strongest increase in the TROPOMI line density over the city (at x = 25 km) is approximately at the centre of Paris, indicating that emissions are likely stronger at the centre than at the edges of the city. Such a spatial variability in the NO_x emissions is indeed suggested in the EDGAR inventory, as shown in Figure 3.2. However, the column model considers the source area as a single homogeneous emission source. In chapter 6 an adapted column model will be applied to account for the effect of spatial emission variability within the city, which has the potential to improve the ability of the model to reproduce the TROPOMI line density.

4.3.2 Estimating the NO_x lifetime

The estimated NO_x lifetime of 3.7 hours for this day in November is relatively short compared to other studies, which found mean NO_x lifetimes of 8.5 (Beirle et al., 2004), 8 (Beirle et al., 2011) and 13.1 hours (Schaub et al., 2007) for wintertime conditions. The case with typical urban conditions at noon of Seinfeld and Pandis (2006), from which the average NO_x/NO_2 is derived, even gives a lifetime of 1.8 days. The short lifetime estimate from the TROPOMI line density could be explained by factors that influence the decrease of the line density beyond the source area. The NO_2 molecules at the downwind end of the line density are emitted hours earlier (for x=200 km at approximately 8:30 hour) when NO_x has a longer lifetime. Indeed, when only equation 4.3 is fitted for $x > x_s$, then the lifetime becomes 8.3 ± 2.07 hours. This raises the question whether the NO_x lifetime is accurately described by equation 4.4 and 4.5.

From Figure 4.2 it is also clear that the column model does not capture all fluctuations in the TROPOMI line density. Diurnal variability in emissions and lifetime are not incorporated in the model, while the emissions are higher (Van der Gon et al., 2006) and the lifetime is longer in the morning (Boersma et al., 2008). A longer lifetime of NO_x in the morning is due to the dependency of its primary sink (reaction 4.2) on the photo-chemical formation of the OH radical (Jacob, 1999). This diurnal cycle in emissions and lifetime is anticipated to lead to a higher line density of NO_2 molecules at the end of the plume compared to a situation with constant emissions and lifetime.

Furthermore, the column model does not account for emissions downwind of the source underneath the passing plume. For instance, the city of Amiens or the A1 highway that runs in the same direction as the line density also add NO_x to the plume. Such downwind emissions that continuously add NO_x to the downwind plume would cause an apparent slower decay, or potentially even local increases, in the line density. Similar to the effect of the diurnal variation in emissions and lifetime, this would lead to a higher estimated NO_x lifetime.

Nevertheless, a different interpretation of the background line density, which is similar to $L_{NO_2}(0)$ in the column model, could have an inverse effect. This background line density is supposed to be constant over the city and along the plume, which would be a valid assumption when it would fully represent the atmospheric background. The number of NO_2 molecules in the tropospheric column above the boundary layer could for instance represent this atmospheric background, because of a longer free tropospheric lifetime due to lower OH concentrations and temperatures compared to the boundary layer. However, figure 4.1 shows that the measured NO_2 columns at $x = 0$ are higher than the minimum further away from Paris. Indeed, the average line density upwind of the source area of Paris for a length of 100 km is 1.2 ± 0.3 $\cdot 10^{22}$ NO_2 molecules cm^{-1}. This indicates that $L(0)$ should not solely be regarded as a constant background, but also as an initial line density from upwind emission sources that enters the city and is immediately subject to chemical decay. When the NO_x loss rate k would be applied to the B term in the column model, then instead of all, only part of the downwind exponential decay would be explained by the first term on the right side of equation 4.5, resulting in a shorter top-down estimated lifetime.

Hence the relatively low NO_x lifetime that was estimated here, is influenced by four effects on the downwind decay that were not accounted for in the column model:

- The diurnal emission cycle
- Variability in lifetime
- Downwind emissions
- Background decay

The first three effects are expected to result in an underestimation of the lifetime and hence an overestimation of the emission, whereas the fourth is anticipated to shown an opposite effect. These influences on the downwind decay will be investigated further in chapter 5.

5 Influences on downwind decay

The previous chapter showed how the emission and lifetime can be estimated from the TROPOMI NO_2 line density. Here the sensitivity of such an emission and effective lifetime estimate to different influences on the downwind decay is tested. Four bottom-up line densities are calculated based on the EDGAR emissions inventory, from which the lifetime and emission are derived with the top-down column model. The reference case uses the total emission for the source area and a predefined lifetime to simulate a line density. The annual average emissions from the EDGAR inventory are multiplied by a factor of 1.3 in order to be representative for a weekday in November around noon (Van der Gon et al., 2011). Four experiments are performed where this reference case is adapted with:

1. Downwind emissions: adding EDGAR's spatial emission pattern and downwind emissions (on average 10% relative to Paris)
2. Diurnal emissions: including 20% higher emissions during rush hour
3. Variability in lifetime: accounting for a 8.3 times lower OH concentration at sunrise than at noon
4. Background decay: applying chemical decay to the background line density

The original column model is then applied in the inverse mode to determine the emission and lifetime from these four simulated line densities. These results are compared to the reference case to determine the sensitivity of the emission and lifetime to these four different influences.

5.1 Methodology

5.1.1 Downwind emissions

The column model assumes a constant emission strength over the source area and that no downwind emission sources are present. To test the sensitivity of emission and lifetime estimates from the top-down column model to this assumption, a bottom-up line density is simulated based on the EDGAR 2012 emission inventory including the emissions downwind of Paris and its spatially variation. This line density is simulated with an adapted form of the column model, where a background line density of $1.7 \cdot 10^{22}$ NO_2 molecules cm^{-1} and a lifetime of 9.8 hours is assumed.

The lifetime of 9.8 hours is calculated with equation 4.3, with an OH concentration of 1.5 $\cdot 10^6$ molecules cm^{-3} (Kanaya et al., 2007), rate constant of $2.5 \cdot 10^{-11}$ cm^3 $molecules^{-1}$ s^{-1} for reaction 4.2 (for surface conditions, Seinfeld and Pandis, 2006) and NO_x/NO_2 ratio of 1.32 (Beirle et al., 2011). This OH concentration is the daytime maximum as observed during the IMPACT IV campaign in central Tokyo from January to February 2004 (Kanaya et al., 2007), which is assumed to be representative for a megacity during winter. Although no OH measurements in Paris for November were available, observations in Paris during the MEGAPOLI campaign in July 2009 (Michoud et al., 2012) show similar values as observations in Tokyo from July to August 2004 (Kanaya et al., 2007), respectively 3.5–10.6 and 6.3 $\cdot 10^6$ molecules cm^{-3}.

The emissions are taken from an emission line density, which integrates the emissions from the EDGAR inventory perpendicular to the wind direction (y) for every x along the wind direction through the centre of Paris, similar to equation 4.1. The emission line density starts 30 km from the centre of Paris and has a total length of 200 km, corresponding the the domain of the TROPOMI

line density in the previous chapter. An emission line density is calculated for each interval (δx) of 7 km, similar to the resolution of the EDGAR inventory of 0.1 by 0.1 degrees (approximately 7 by 11 km). Since the EDGAR emissions are reported as mass of NO_x, these numbers are converted to NO_x molecules with the molecular weight of NO_2, as specified in the EDGAR data set. The resulting emission line density is shown in figure 5.1, showing a clear emission peak over Paris and 10 times lower downwind emissions. The exact origin of the peak around x = 175 km could not be found, since there is not city or other large emission source at this location (50.15N 2.65E in Figure 3.2).

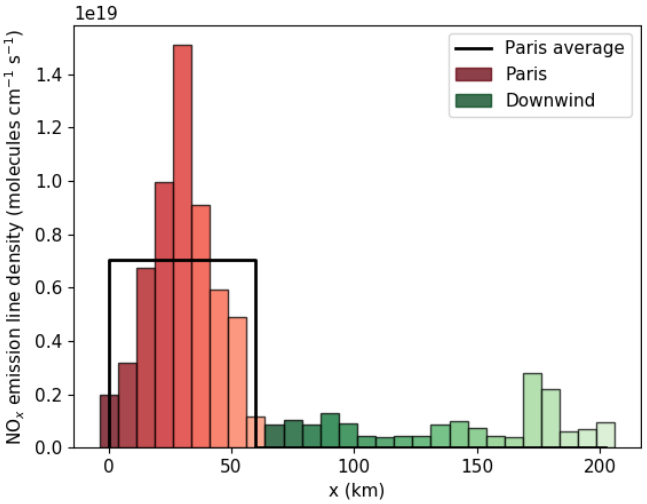

Figure 5.1: Emission line density from the EDGAR NO_x emission inventory along the wind direction (x) from 2012 and the average EDGAR NO_x emission for Paris and zero downwind emissions.

For all n emissions (E_i) at x_i on the emission line density, a NO_2 line density is simulated, which is shown in Figure 5.2. In contrast to Jacob's column model (1999), which has a source area from 0 to x_s, in this approach the source area runs from $x_i - \frac{\delta x}{2}$ to $x_i + \frac{\delta x}{2}$ for each emission on the emission line density, which correspond to the approximate grid size of the EDGAR inventory (δx = 7 km). The line density L_i for E_i as a function of x is then given by the following three formulas:

$$L_i(x, E_i) = 0 \text{ for } 0 \leq x < x_i - \frac{\delta x}{2} \tag{5.1}$$

$$L_i(x, E_i) = \frac{E_i}{k}\left(1 - e^{-\frac{k(x - x_i + \frac{\delta x}{2})}{U}}\right) \text{ for } x_i - \frac{\delta x}{2} \leq x \leq x_i + \frac{\delta x}{2} \tag{5.2}$$

$$L_i(x, E_i) = L_i(x_i, E_i)e^{-\frac{k(x - x_i - \frac{\delta x}{2})}{U}} \text{ for } x > x_i + \frac{\delta x}{2} \tag{5.3}$$

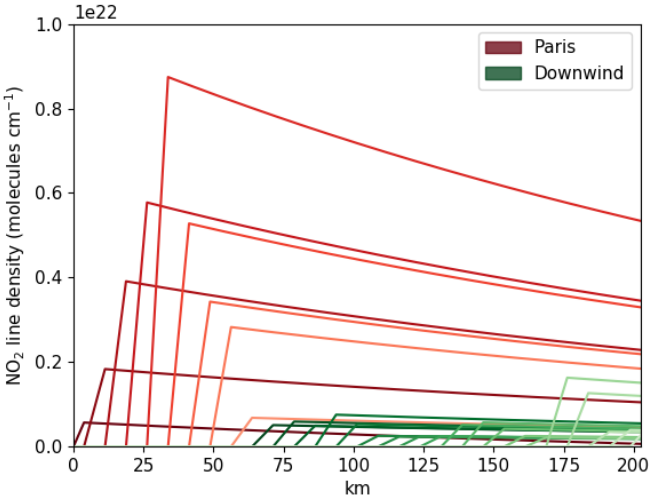

Figure 5.2: All n simulated NO_2 line densities for each E_i on the emission line density, where red depicts the line densities for emission from Paris ($x \leq x_s$) and green the line densities for downwind emissions ($x > x_s$).

All the resulting simulated line densities for each E_i are then summed to obtain the total bottom-up line density:

$$L(x) = \sum_{i=1}^{n} L_i(x, E_i) + B \tag{5.4}$$

Finally, the inverse method is used to obtain an estimate for the emission and lifetime by fitting the column model functions to the simulated bottom-up line density, which are compared with the initially assumed lifetime of 9.8 hours and the temporally corrected spatially averaged emission over Paris (70.3 mol NO_x s^{-1}, from chapter 4). An uncertainty of 50.7% in the simulated line density is used, based on the uncertainty in the EDGAR emission inventory (Crippa et al., 2018).

5.1.2 Diurnal emissions

The column model implicitly assumes that the emission source is continuous. In reality, Paris' NO_x emissions follow a diurnal cycle, with strongest emissions during rush hour. This can be seen in the observed NO_2 concentrations at the top of the Eiffel Tower, as shown in Figure 5.3 for 22 November 2017, where the concentrations during rush hour are approximately 20% higher than around noon. Similar to the Eiffel Tower observations, the temporal emission pattern from the TNO report by van der Gon et al. (2011) gives 18% higher rush-hour emissions (7.00 to 9.00 UTC) compared to noon (Figure 5.3). In this third experiment, this pattern is used to scale the EDGAR emissions in the column model:

$$E(t) = E_{\mathrm{EDGAR}}(13h) \cdot \frac{E_{\mathrm{TNO}}(t)}{E_{\mathrm{TNO}}(13h)} \text{ with } t(x) = \frac{x - x_s}{U} \tag{5.5}$$

From the resulting new line density, the emission and lifetime of NO_2 is derived with the inverse column model to assess the influence of temporal emission variability on those two parameters.

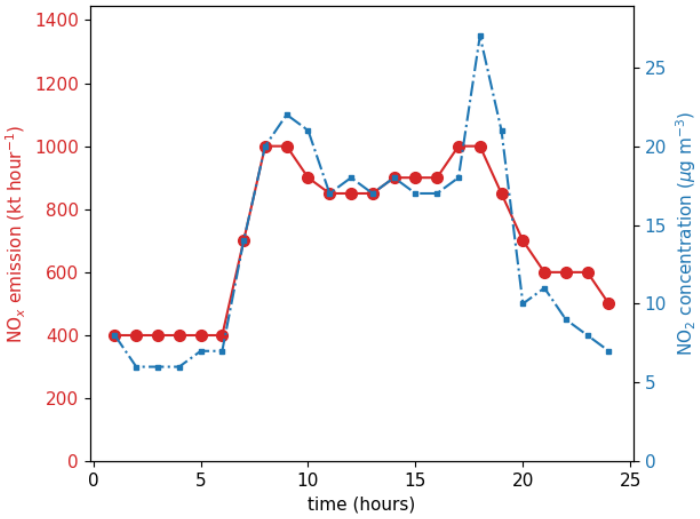

Figure 5.3: Diurnal cycle in NO_x emissions from the EDGAR inventory with temporal correction and NO_2 concentration observed on 300 m at the Eiffel Tower in Paris on 22 November 2017.

5.1.3 Variability in lifetime

Similar to the previous experiment on the diurnal emission cycle, also the lifetime varies throughout the day. During daytime, the NO_x lifetime is determined by the oxidation with OH to HNO_3, as described by reaction 4.2. Since the formation of OH requires solar radiation, τ_{NO_x} is shortest around noon and longest at dawn. Similar to NO_x lifetime derivation in paragraph 5.1.1 and because no OH observations in Paris on 22 November 2017 were available, figures from the IMPACT campaign in Tokyo are used that gives an OH concentration of 0.18 $\cdot 10^6$ molecules cm^{-3} during nighttime (Kanaya et al., 2007). This is 8.3 times lower than the maximum daytime OH concentration. Although it is likely that the OH concentration in Paris on 22 November 2017 would be different from these observations over Tokyo from January to February 2004, the diurnal variation should give a good representation of the variation in lifetime, and hence the sensitivity of the estimated column model parameters.

Since the TROPOMI observations consist mainly of NO_x emitted in the hours before its early-afternoon overpass time, the linear change in OH concentration per unit of time ($\frac{\delta[OH]}{\delta t}$) is given by the difference between the OH concentration at noon (12.36 UTC) and at dawn (8.10 UTC) over the difference in time. Before dawn and after noon the OH concentration is kept constant. Based on equation 4.3 the variable rate constant k_v is implemented in the model with the following formula as a function of dt, which is the time before the TROPOMI overpass time in seconds:

$$k_v(dt) = \frac{k_2([OH]_{\text{noon}} - \frac{\delta[OH]}{\delta t} dt)}{[NO_x]/[NO_2]} \tag{5.6}$$

This results in a NO_x lifetime of 81.5 hours at dawn and 9.8 hours at noon, shown in Figure 6.2. This figure runs from the TROPOMI overpass time at 12.52 back to 7.05 UTC, since part of the end of the plume (x = 200 km) is emitted 5.8 hours earlier (x/U).

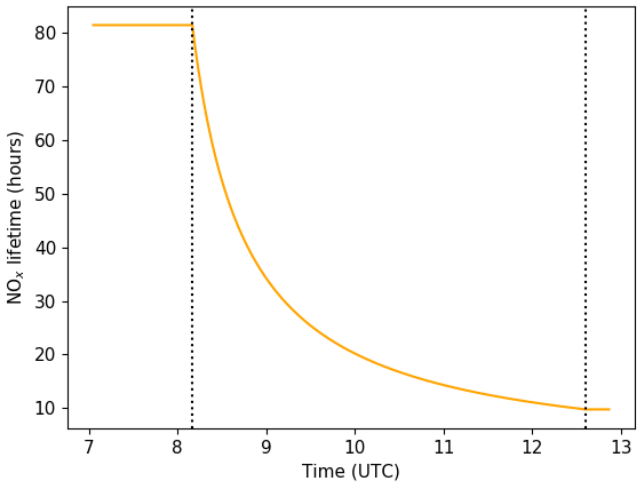

Figure 5.4: Variability in NO_x lifetime for wintertime conditions, decreasing from sunrise (8.10 UTC, dotted line) to solar noon (12.36 UTC, dotted line) from the morning until the TROPOMI overpass time.

Because the column model by Jacob (1999) considers the chemical decay to be constant, the lifetime as a function of t is implemented into the derivatives of equation 4.4 and 4.5. These derivatives describe the change in the line density per distance along the wind direction ($\frac{dL}{dx}$). This change is determined by the emission (E) for $x \leq x_s$ and the chemical decay ($k \cdot L$) as a function of x_i and x. The variable x_i denotes the location of the derivative of L, whereas x defines the location of L once it is observed by TROPOMI, so that $\frac{x_i - x}{U}$ is dt, the time that it would take for the line density at x_i to reach x. In other words, each line density as observed at 12.52 UTC would at an earlier time (12.52 UTC - dt) be located at x_i where it would shrink because of chemical decay and, if located over the source area, grow because of emissions. This is described by the following two equations, with $dt = \frac{x_i - x}{U}$:

$$\frac{dL}{dx}(x_i, x) = \frac{E - k_v(dt) \cdot L(x_{i-1})}{U} \text{ for } 0 \leq x \leq x_s \tag{5.7}$$

$$\frac{dL}{dx}(x_i, x) = \frac{-k_v(dt) \cdot L(x_{i-1})}{U} \text{ for } x > x_s \tag{5.8}$$

The line density (L) as a function of x at $dt = 0$ is then given as the sum of each derivative at x_i up to $x_n = x$:

$$L(x) = \sum_{i=1}^{n} \frac{dL}{dx}(x_i, x) \cdot (x_i - x_{i-1}) \text{ where } 0 \leq x_i \leq x \tag{5.9}$$

Similar to the previous two experiments, the simple column model is inversely applied to obtain estimates for the emission, lifetime and background line density. These figures are subsequently compared to the reference case and the other experiments to determine the sensitivity of these estimated parameters to lifetime variability.

5.1.4 Background decay

As the emission and lifetime term in the column model are evaluated in the previous three experiments, this last and fourth experiment focuses on the background component (B). From the TROPOMI line density from 22 November 2017, the column model estimates the line density to

be 1.6 $\cdot 10^{22}$ NO_2 molecules cm^{-1} (Table 4.1). However, by looking at both the TROPOMI and fitted column model functions, it appears that the background line density is mainly determined by the initial line density at x = 0 km. This raises the question whether this value truly represents the background.

The variability in the upwind line density could be explained by a different regional background level, but also partly by upwind emission sources. When the background line density would originate completely from upwind emissions, then it should rather be seen as an 'initial' line density, which chemically decays as it moves along with the wind. This interpretation is implemented in the model as follows:

$$L_{NO_x}(x) = \frac{E}{k}\left(1 - e^{-\frac{kx}{U}}\right) + Be^{\frac{-kx}{U}} \text{ for } 0 \leq x \leq x_s \tag{5.10}$$

$$L_{NO_x}(x) = L_{NO_x}(x_s)e^{-\frac{k(x-x_s)}{U}} + Be^{\frac{-kx}{U}} \text{ for } x > x_s \tag{5.11}$$

Although it seems probable that at least part of the background line density of 1.7 $\cdot 10^{22}$ NO_2 molecules cm^{-1} originates from upwind emission sources, this part would be difficult to distinguish from the component that is uniform in space. This spatially uniform part could be the result from an error in the partitioning between the tropospheric and stratospheric column.

In this experiment, the full background component is decaying as it moves in the x direction. The resulting simulated density in combination with the column model is used to estimate the three parameters E, k and B, to test how sensitive this approach is to the assumption that the background component remains constant.

5.2 Results

When downwind emissions are added to the column model, the simulated line density for experiment 1 shows a weaker decay downwind of the source area (Figure 5.5a). At the end of the plume, almost one third of the line density originates from downwind emissions. When the original column model is fitted to the line density with downwind emissions, the resulting NO_x lifetime is longer. Hence neglecting downwind emissions leads to an overestimation of the lifetime. Interestingly, the higher lifetime in this experiment does not lead to a lower emission. While E is 3.7 mol s^{-1} higher than the reference case (Table 5.1), the opposite would be expected, since a similar change in magnitude requires a larger E when k becomes smaller ($\frac{dL}{dt} = E - kL$). Yet it appears that this effect is compensated with the lower estimated background line density by the fitted column model. This lower value for B leads to a better fit over the source area, since the simulated line density has an S-shape, with the strongest increase over the middle of the city.

Similar to the result of adding downwind emissions, experiment 2 with a diurnal emission cycle shows a higher lifetime. Because the effect of the spatial distribution in emissions over the source area does not play a role here, the NO_x emission is estimated to be 4.5 mol s^{-1} smaller than the reference case (Table 5.1). The simulated line density, shown in Figure 5.5b, is higher at the end of the plume, because this part originates from rush-hour NO_x emissions. This results in a lifetime that is 6.2 hours longer.

Accounting in the model for a variable lifetime in experiment 3 gives a quite similar effect as the diurnal emission cycle. Since earlier emissions have a longer lifetime, the end of the simulated NO_2 line density becomes larger (Figure 5.5c). The lifetime that is obtained from applying the inverse column model is 7.1 hours longer, and the emission 3.7 mol s^{-1} smaller compared to the reference case (Table 5.1).

In contrast to the the previous three experiments, experiment 4 gives a lower line density because a decay factor is applied to the background parameter (Figure 5.5d). The resulting estimated

lifetime is 4.3 hours shorter and the emission 1.1 mol s^{-1} smaller than the reference case (Table 5.1).

Table 5.1: Column model estimates and standard deviation of NO_x emission, lifetime and background line density fitted to the line densities of the four experiments, in comparison to the reference case.

Experiment	Emission (mol s^{-1})	Lifetime (hours)	Background ($\cdot 10^{22}$ molecules cm^{-1})
Reference	70.3 ±11.35	9.8 ±4.27	1.7 ±0.22
1. Downwind emissions	74.0 ±10.59	29.3 ±31.14	1.5 ±0.22
2. Diurnal emissions	65.8 ±22.37	16.0 ±22.22	1.7 ±0.48
3. Variable lifetime	66.6 ±22.40	16.9 ±24.44	1.7 ±0.48
4. Background decay	69.1 ±12.16	5.5 ±1.69	1.7 ±0.22

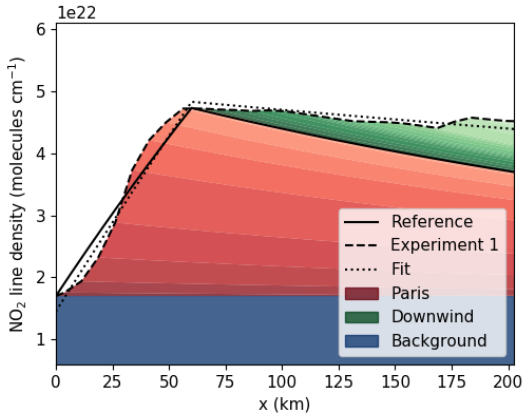

(a) Experiment 1: downwind emissions

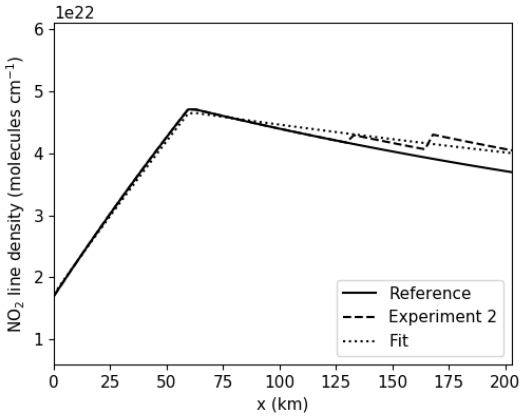

(b) Experiment 2: diurnal emissions

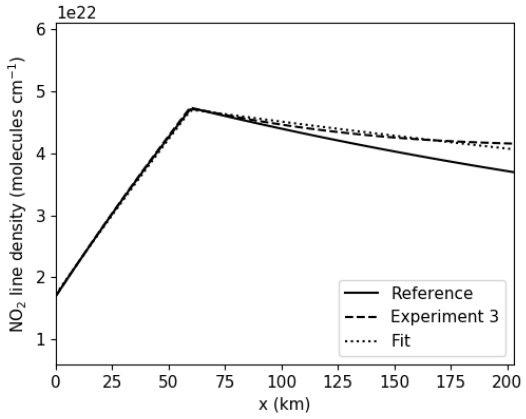

(c) Experiment 3: variable lifetime

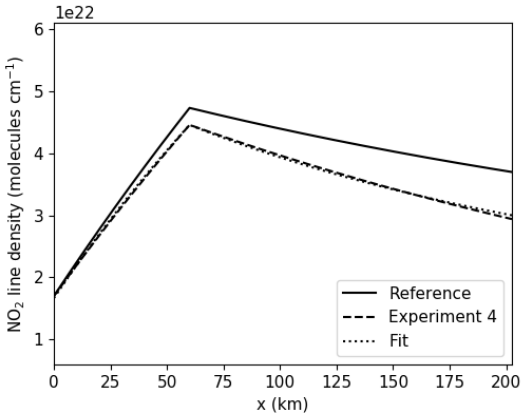

(d) Experiment 4: background decay

Figure 5.5: The simulated line densities of the reference case, the four experiments and the inverse column model that is fitted to obtain estimates for the emission, lifetime and background line density.

5.3 Discussion

The four different experiments show how the estimated NO_x emission, lifetime and NO_2 background line density are influenced by spatial and temporal variability in emissions, addition of emissions to the downwind line density and background decay. Accounting for downwind emissions in experiment 1 leads to the largest difference in lifetime compared to the reference case, namely 3.0 times longer. Although one would expected that this longer lifetime results in a lower emission based on the column model equations, experiment 1 gives a higher emission than the reference case because the fit adapts to the spatial emission pattern by lowering the background line density. When this effect is excluded by keeping B constant in the fit, then an emission of 65.3 $\pm$ 7.08 mol s^{-1} is estimated from the simulated line density with downwind emissions. Hence even a very large overestimation of the lifetime by a factor of 3.0 due to downwind emissions results in a relatively small underestimation of the emission by 7.1%.

This finding that a relatively large overestimation in lifetime results in a slight underestimation in emission is confirmed in experiment 2 and 3, which give respectively a 6.4% and 5.3% lower emission compared to the reference case. In comparison, the study by Beirle et al. (2011), which estimated NO_x emissions and lifetimes for multiple megacities from line densities based on averaged satellite observations for multiple years, also concludes that "possible different nighttime behaviour of τ and E has almost no impact" on their estimated parameters (supporting online material, p. 6). Similar to experiment 2, their simulation with 10 times lower nighttime emissions leads to approximately 10% higher emissions, and similar to experiment 3, their estimated emission is approximately 10% lower from a simulated line density with a 10 times higher nocturnal lifetime (Beirle et al. 2011).

Beirle et al. (2011) also found that the lifetimes obtained from the fits to the simulated line density with longer lifetimes and lower emissions during the night deviate less than two hours from their default lifetime of 5 hours. Although the differences in lifetime between experiment 2 and 3 with the reference case are much larger than Beirle et al. (2011), this can be explained by the shorter initial lifetime of 5 hours compared to 9.8 hours. When experiment 2 and 3 are performed again, but with a doubled OH concentration that corresponds to a lifetime of 4.8 hours, the difference in lifetime is in the same order of magnitude, namely 1.0 and 3.5 hours longer.

However, the large differences in NO_x lifetime estimates between the four experiments and the reference case show that it remains difficult to get an accurate estimate with fitting an exponential function through the downwind decay in a line density. The experiments presented here could be combined to improve the column model and potentially enable a more accurate lifetime estimation.

Besides improving the model to obtain a better lifetime estimate from the downwind line density, it might also be an option to obtain an OH concentration from other sources, such as the CAMS model, to calculate the NO_x lifetime. When the lifetime is not estimated from the line density, the emission can be estimated solely from the line density over the source area. Downwind emissions, the diurnal emission cycle and variability in lifetime would then not influence the estimated emission with the column model anymore. An effect that should be considered is the spatial variability in emissions over the city, as that has shown to have a large influence in experiment 1. This approach will be evaluated in the next chapter, where an emission will be estimated with the column model just from the increase in line density over Paris.

6 Accumulation over the source area

In chapter 4, it is shown how the column model as described by Jacob (1999) can be used to derive the NO_x emission and lifetime from a line density of TROPOMI observations. Because chapter 5 proved the large effects in the downwind component of the line density on the column model lifetime estimates, this sixth chapter evaluates the accumulation of NO_2 just over Paris in the wind direction.

Besides the TROPOMI observations of 22 November 2017, two longer periods from 22 to 26 February and from 17 to 24 April 2018 are evaluated. In these periods three days were excluded, as described in paragraph 3.5. Firstly, the TROPOMI observations are validated by comparing the surface NO_2 measurements in Paris with the line density for each of the 11 days to test whether or not the built-up of NO_2 in the wind direction can also be seen in the surface observations. Secondly, the emission is estimated just from the TROPOMI line density over the source area with a column model as well as an adapted column model that incorporates the spatial emission pattern within the city, both with a simulated NO_x lifetime from a chemical transport model.

This new approach, where the the downwind decay component is disregarded and the NO_x emission is estimated just from the accumulation over the source area, would be an optimal use of increased resolution of TROPOMI compared to previous instrument. Indeed, from Figure 6.2 one can see that the source length x_s of Paris encompasses eight TROPOMI observations, which is also reflected by the strongest increase in the line density over the middle of the city.

6.1 Methodology

6.1.1 Comparison with surface observations

To compare the surface observations with the TROPOMI line density, the distance x along the wind direction is calculated for each observatory. The resulting observed NO_2 concentrations as a function of x are then averaged for each interval on the TROPOMI line density, if the difference in distance x between the surface observation and TROPOMI line density is smaller than 3.5 km (half of the integration interval of the TROPOMI line density). This average is then compared with the TROPOMI line density, to validate that this pattern is also visible in the measured surface concentrations.

6.1.2 Estimating emission from source area accumulation

In order to test whether the NO_x emission can be estimated just from the accumulation over Paris based on the TROPOMI line density, the column model is applied, similar to the method described in chapter 4 but now focusing on the source area. In other words, just equation 4.4 of the column model is applied.

Since the lifetime cannot be estimated from the decline downwind of the source area, predefined lifetimes are assumed (Table 6.1). The NO_x lifetime for 22 November 2017 is 9.8 hours, as used in chapter 4 and 5. The lifetimes for the days in February and April 2018 are taken from Lorente et al. (unpublished paper, 2018), which is based on Equation 4.4, the mean boundary layer concentration of NO_x, NO_2 and OH simulated by the CAMS model over Paris at noon and a rate constant (k_2) of 2.6 $\cdot 10^{-11}$ cm^3 $molecule^{-1}$ s^{-1}. Because 19 April was not included in this study, the average lifetime from the other days in April was taken here. The assumed lifetimes show a strong difference

between February and April because of more solar radiation that is required for the formation of OH.

It should also be noted that the sounding observations of wind speed and direction at Trappes (Table 3.1), which are used to derive the line densities and estimate emissions with the column model, were unavailable for 22 February, 23 February and 22 April. Wind date for these data is supplemented by Lorente et al. (unpublished paper, 2018), whom calculated the mean wind for the boundary layer at 12.00 UTC from the 6-hourly ECMWF-Interim reanalysis.

Table 6.1: Predefined NO_x lifetimes used to estimate emission with the column model from the line density over the source area.

Month	November 2017	February 2018				April 2018					
Day	22	22	23	25	26	17	18	19	21	22	24
NO_x lifetime (hours)	9.8	16.0	10.9	11.4	10.3	1.6	2.0	2.6	2.9	2.7	2.8

6.1.3 Spatial column model for emission pattern over the source area

The TROPOMI line density of 22 November 2017, illustrated in Figure 4.3 from chapter 4, showed the strongest increase over the centre of Paris. Indeed, also the bottom-up simulated line density of experiment 1 in chapter 5, which included the spatial distribution in emissions from the EDGAR inventory, showed an S-shape with the strongest increase of NO_2 in the x direction over the centre of the source area. This hints that including the spatial emission pattern in the column model would result in a better fit with the TROPOMI line density, and hence a more accurate emission estimate.

To test this assumption, and adapted form of the column model accounting for the spatial emission variability is used to estimate emissions. A large number of line densities is simulated for a large number of different total emission strengths, of which the estimate is the emission corresponding to the simulated line density with the lowest χ^2 (Equation 4.6) compared to the TROPOMI line density.

The line densities are simulated similarly to the method described in section 4.1.1, where the simulated line density is the sum of the line densities for each emission at distance x on the emission line density. This is described by Equation 5.11. The emission line density is based on the EDGAR inventory, and averaged for all wind directions with intervals of 10 degrees (Figure 6.1).

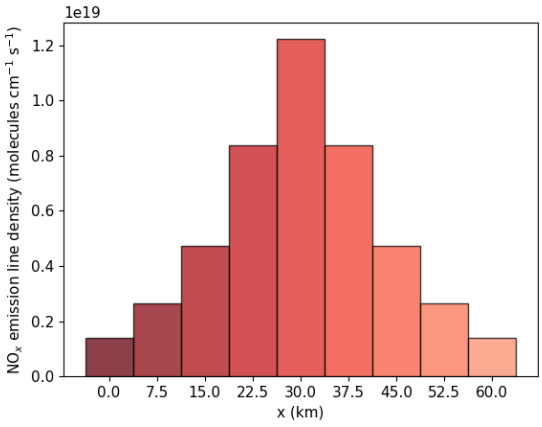

Figure 6.1: NO_x emission line densities averaged for all directions.

6.2 Results

The tropospheric NO_2 columns measured by TROPOMI show an increase in the wind direction, as illustrated in Figure 6.2 and 6.3, for all days that were analysed, except 22 April 2018. On this day it is difficult to notice a trend over the domain of the city, although higher columns can be seen downwind (northeast) of the city. These figures also show that the wind direction that is used corresponds well with the direction of the NO_2 plume that is observed with TROPOMI; for most days both point in the same direction. For two days, however, one can note a slight deviation between the wind's and plume's direction. On 22 February 2017 the plume is pointed more towards the south and on 21 April 2018 the direction of the plume is tilted towards the north, in comparison with the direction of the wind. Yet this does not appear to be a problem for the line density derivation, since the full width of the plume is still covered within the domain of the line density at the end of the source area (x=60 km).

The surface NO_2 measurements show a similar pattern as TROPOMI's NO_2 columns: higher values closer to the centre and at the downwind side of the city. This is shown in Figure 6.3 for all days in February and April 2018, and in Figure 6.2 for 22 November 2017, since this day has higher surface NO_2 concentrations compared to the other days and therefore requires a different scaling. When comparing all days in Figure 6.3, it becomes clear that also the magnitude of measured NO_2 correspond between the surface concentrations and tropospheric columns. For instance 22 April 2018, when both TROPOMI and surface measurements give low values. In addition, for most days also the measured surface concentrations averaged at distance x show an increase similar to the TROPOMI line densities (Figure 6.5). However, this is not the case for 19 April 2018, perhaps due to the comma-shape of the downwind plume (Figure 6.3) that is caused by turning wind (from 160 at 8.00 UTC to 220 at 13.00 UTC at the surface station in Trappes), 21 April 2018, where one single station around x=47 km lowers the average value at the downwind side of the city, and 24 April 2018, which hints at an error in the TROPOMI observations that are unexpectedly low over the centre of Paris. Nonetheless, it can be concluded that overall the increase in NO_2 abundance over the city of Paris in the wind direction is not only observed by TROPOMI, but also by surface observations.

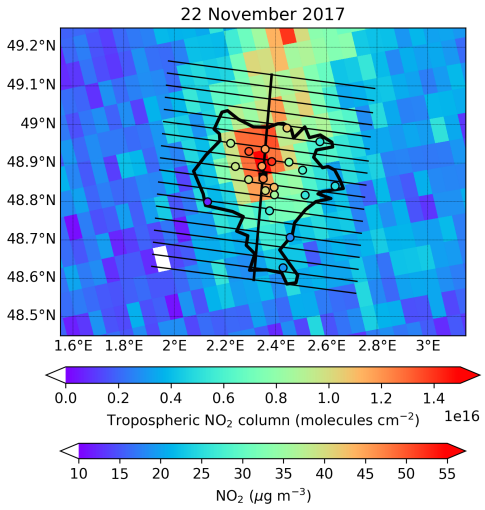

Figure 6.2: Measured tropsopheric NO_2 column by TROPOMI and surface observations on 22 November 2017. The thick line denotes the wind direction (x) and the thin lines with intervals of 3.5 km represent each line density for which all pixels perpendicular to the x direction are integrated.

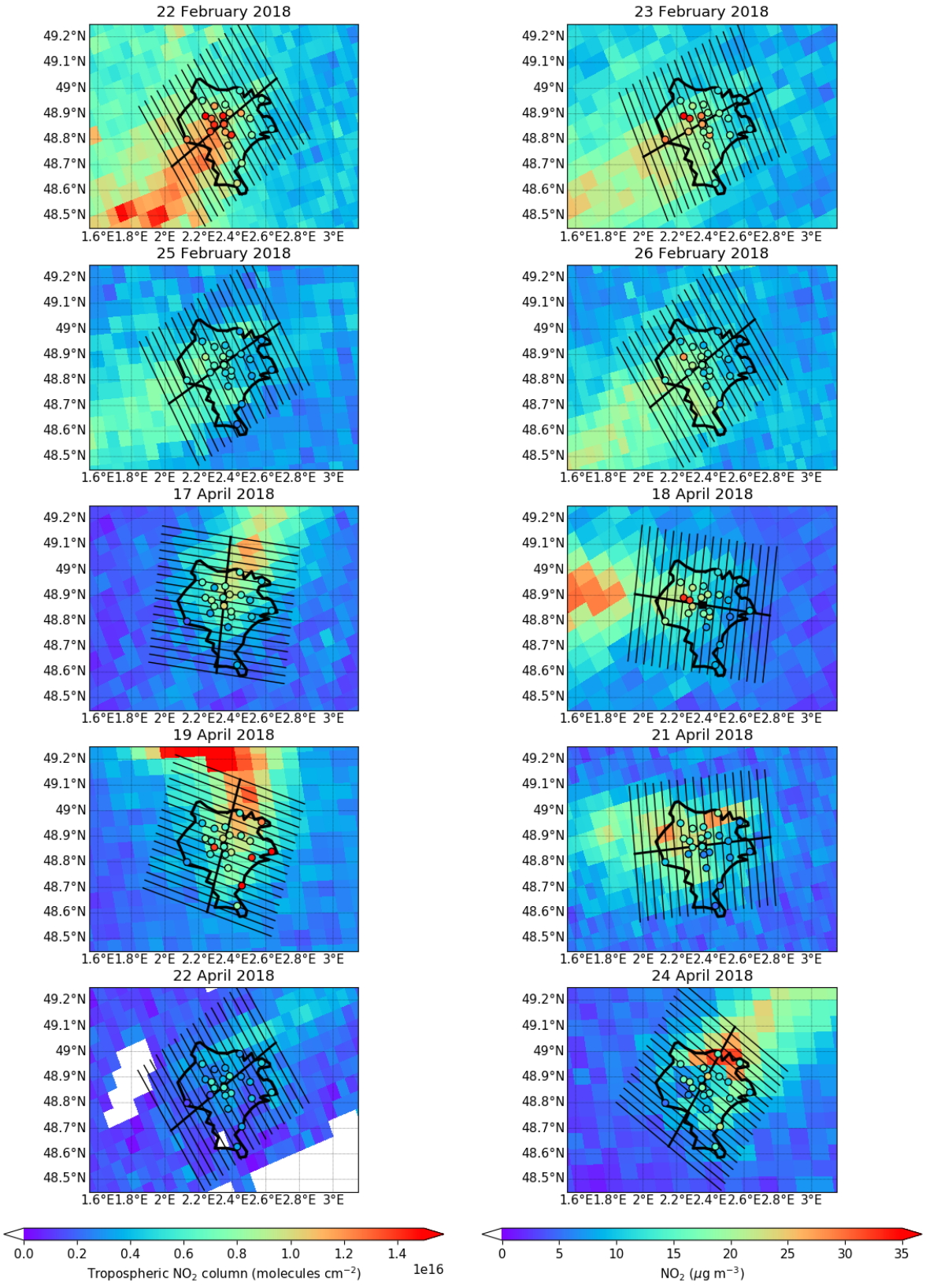

Figure 6.3: Measured tropsopheric NO_2 column by TROPOMI and surface observations for the two periods in February and April 2018. The thick line denotes the wind direction (x) and the thin lines with intervals of 3.5 km represent each line density for which all pixels perpendicular to the x direction are integrated.

Since the surface observations validate the trend in the TROPOMI line density, the next step is to estimate the NO_x emissions from the TROPOMI line density with both the column model and spatial column model, the latter accounting for the spatial emission pattern. After fitting the column model functions to the TROPOMI line density (Figure 6.5), the resulting NO_x emission estimates from the column model are higher or almost the same as the spatial column model for most days (Table 6.2). For about half of the analysed days, namely all days in February 2018 and both 17 and 19 April 2018, the spatial column model has lower χ^2 values, indicating a better fit to the TROPOMI line density than the column model without the spatial emission distribution. Indeed, for these days the TROPOMI line densities show a clear symmetrical S-shape, while the days where the spatial column model performs worse show some decline at the downwind side of the city. Thus, in contrast to the hypothesis based on the discussions of the results from chapter 4 and 5, it cannot be concluded that including spatial variation of emissions from the EDGAR inventory within the source area in the column model, while using a predefined lifetime, leads to an improvement.

When interpreting the emission estimates from Table 6.2, it is good to note that ERA-Interim wind data was used for 22 and 23 February 2018, as well as 22 April 2018. The wind speeds for these days appears to be higher, in comparison to the sounding observations and surface wind measurements (Table 3.1). According to the column model equations, a higher wind speed would result in a lower emission. This could partly explain that 22 April 2018 is the lowest estimated emission. In contrast, the two days in February are actually at the higher end of the emission estimates.

Table 6.2: Emission estimates for all days with the column model and spatial column model and the respective χ^2 value for the model fit with the TROPOMI line density.

Date	Day	Column model		Spatial column model	
		Emission (mol s^{-1})	χ^2	Emission (mol s^{-1})	χ^2
22/11/17	Wednesday	60.2	25.5	56.6	28.5
22/02/18	Thursday	67.7	24.7	58.2	3.3
23/02/18	Friday	59.3	18.1	51.8	4.7
25/02/18	Sunday	31.2	11.2	30.1	7.5
26/02/18	Monday	51.5	30.7	43.2	17.5
17/04/18	Tuesday	59.3	44.2	54.6	6.1
18/04/18	Wednesday	68.1	18.1	68.6	33.0
19/04/18	Thursday	50.7	26.3	46.1	21.4
21/04/18	Saturday	38.7	12.9	35.8	15.4
22/04/18	Sunday	29.3	19.0	25.4	24.6
24/04/18	Tuesday	48.4	15.2	51.7	43.0

From the magnitude of the emissions for each day of the week, illustrated in Figure 6.4, it becomes clear that the NO_x emissions during the weekend are half as large as during weekdays (54% for both the column model and the spatial column model). The standard deviations of these averages are all quite low, where the highest standard deviation is 9.0 mol s^{-1} for the column model emission estimates during weekdays.

The estimated NO_x emissions are also substantially lower then the averaged emission from the EDGAR inventory for Paris from 2012 with a correction for temporal variation of 4.7% for winter, 19.3% for noon, 6.1% for weekdays and -15.2% for weekends (van der Gon et al., 2011). This

results in an average NO_x EDGAR emission for Paris is 73.1 mol s^{-1} for weekdays and 61.1 mol s^{-1} for the weekend. In comparison, the column model estimated NO_x emission is respectively 24% and 51% lower than the temporally corrected EDGAR emissions. Also the difference between weekday and weekend emissions is much larger in the average column model estimates: 2.0 times for the column model and just 1.2 times for the EDGAR inventory.

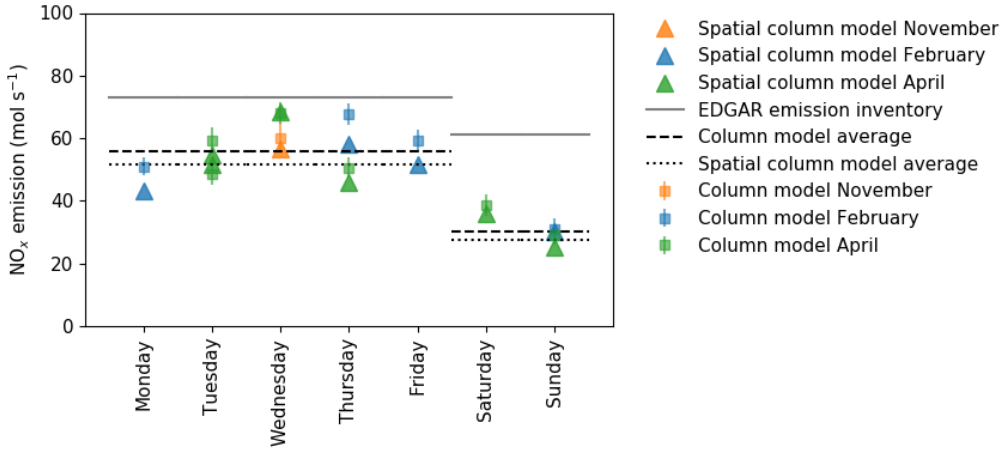

Figure 6.4: Emission estimates for Paris with the column model and spatial column model from the TROPOMI line densities for 22 November 2017 and the two periods in February and April 2018, as well as the average for weekdays and weekend in comparison to the emission from the EDGAR inventory with temporal correction.

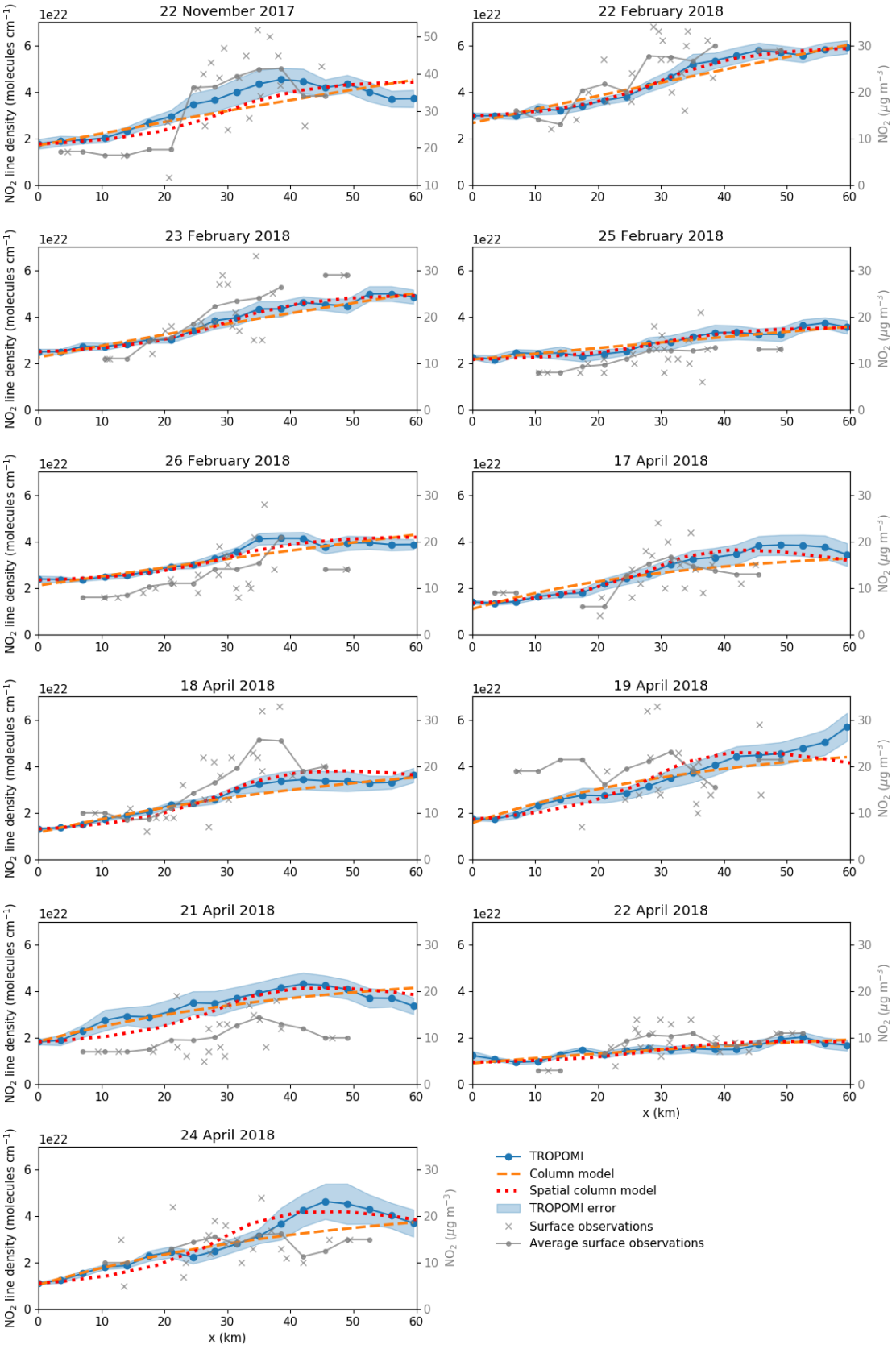

Figure 6.5: NO_2 line densities over Paris from TROPOMI, measured surface concentration and column model fits.

6.3 Discussion

This sixth chapter showed how the NO_x emission from Paris can be estimated just from the accumulation over the city, which is now possible because of the higher resolution of TROPOMI in comparison to its precessors. Previous studies such as by Beirle et al. (2011) required satellite NO_2 observations beyond the scope of the source domain to determine the NO_x lifetime from the downwind decay. However, as shown in chapter 5, this approach adds complexity since downwind emissions and variability in time influence the estimated NO_x lifetime, processes that are not considered in the column model as introduced in chapter 4. These processes do not pose a problem when the NO_x emission is estimated from the increase in NO_2 abundance over the city and the NO_x lifetime is obtained in a different way. Although the use of a lifetime from a chemical transport model brings in another uncertainty, the effect of chemical decay is only minor[1] compared to the increase due to emission. This was also confirmed in chapter 5, which concluded that even a large overestimation of the lifetime leads to only a small underestimation of the emission.

Besides the advantage that influences on the downwind plume do not perturb the emission estimate when applying the column model just to the source area, this new approach also has a second advantage. Whereas previous efforts to estimate NO_x emissions with satellites relied on averaged data, often for multiple years, to get a sufficiently fine resolution, here daily emission estimates can be made just from a single TROPOMI overpass. This makes it possible to analyse seasonal and diurnal emission patterns, which can lead to a better understanding of contributions from different emission sources and hence the effectiveness of climate change and air quality mitigation strategies.

The weekly cycle of NO_x emissions from the column model estimates for eleven analysed days showed a factor of 2.0 higher emissions during weekdays than the weekend. This is a much stronger differences than the report by van der Gon et al. (2011), which differ by a factor of 1.2. One would expect lower NO_x emissions during the weekend, as there is less traffic than during the week. The lower difference in the temporally corrected EDGAR inventory could hence hint at a too high emission factor for traffic or an underestimation of traffic numbers in the activity data.

Not only is the weekly variation stronger, also the average NO_x emissions during weekdays and weekend of the estimates from the TROPOMI line density are well below the average reported emissions of the temporally corrected EDGAR inventory (respectively 24% and 51%). This could mean that the NO_x emissions reported in the EDGAR inventory are too high. However, one should note that the EDGAR inventory from 2012 is used. The tri-annual mean NO_2 concentration decreased by about 8% at background sites in Paris from 2011-2013 to 2015-2017 (Airparif, 2018). Also the European Environmental Agency reports a decrease in NO_x emissions by 15% for France from 2012 to 2016 (EEA, 2017). This emission reduction could could explain to a certain extend the lower TROPOMI emission estimates compared to the EDGAR inventory of 2012.

However, directly comparing NO_x emission figures from the top-down estimates based on TROPOMI observations with those from the bottom-up reported EDGAR emission inventory requires caution. As mentioned before, the former is representative for the emissions around midday, whereas the latter is an annual average that can be corrected with temporal correction factors. No temporal correction factors are available from the EDGAR inventory. And it is likely that the factors used in this study from a TNO report (van der Gon et al., 2011) have a high uncertainty embedded. For instance, the diurnal cycle in emissions from road transport is based on traffic intensity time series from 1985 to 1998 in the Netherlands. It seems plausible that not only traffic intensity and emission abatement in cars decreased in the past decades, but also that the temporal variation in Paris is different than in the Netherlands.

[1] The chemical decay rate is 7% of the emission according to $\frac{kB}{E}$, with k and B based on the lifetime and background used in chapter 5 and E as the average EDGAR emission over Paris from figure 5.1.

Furthermore, not only the limitations of the temporal correction factors require attention, but also the TROPOMI NO_x estimates. Firstly, the accuracy of the tropospheric NO_2 columns as observed by TROPOMI needs to be considered. Although the validation with the surface NO_2 measurements in Paris aligns well with both the variation in space and magnitude of the TROPOMI observations, a further validation would be recommended, for instance with ground-based MAX-DOAS measurements.

Secondly, the wind speed is an important parameter in the column model and has a large influence on the estimated NO_x emission. When wind speeds are halved, which corresponds on some days to the difference between the wind speed at the surface and middle of the boundary layer (Table 3.1), the column model NO_x emission estimates are on average 40% lower then the values presented in Table 6.2. In order to determine a more accurate wind speed for the column model, it would be useful to have a better understanding of the vertical profile of NO_2, since wind speed increases with altitude.

Thirdly, the chemical decay in the column model needs to be considered. A disadvantage of applying the column model over the city is that estimating the NO_x lifetime from the TROPOMI line density would be difficult as the signal is minor compared to the emissions. Hence lifetimes are needed from CAMS model simulations (unpublished paper, Lorente et al., 2018), whom report an uncertainty of 50% for these lifetimes. When the lifetimes as described in Table 6.1 are lowered by 50%, the column model emission estimates are on average 21% higher then the values in Table 6.2. However, a limitations to the results from this chapter is the conversion from NO_2 to NO_x. This is done with the NO_x/NO_2 ratio, which is assumed to have a constant value of 1.32, while the Eiffel Tower observations give an average ratio of 1.79 for four days in February 2018 and 1.40 for five days in April 2018. Applying these higher NO_x/NO_2 ratio to the column model would lead to a higher emission.

And lastly, accounting for the spatial emission pattern in the column model, with the steepest increase in line density over the centre of the source area, does only lead to a better fit (lower χ^2) for some days. It seems that, except for 22 November 2017 and 17 April 2018, especially on days with higher wind speeds the spatial column model performs better then the simple column model. Perhaps this is due to the fact that chemical loss becomes relatively more important at lower wind speeds.

7 Conclusion

The improved resolution of the new TROPOMI satellite measurements now enables us to see how the abundance of NO_2 in the troposphere accumulates over a large source area, such as the city of Paris, and decays downwind. This evolution of NO_2 in the direction of the wind can be described by the TROPOMI line density, from which the NO_x emission, lifetime and background can be estimated with a simple column model for a single day. After applying this method to the TROPOMI observations of 22 November 2017, the resulting estimated NO_x is just 6% higher than the EDGAR emission inventory when a temporal correction factor is applied. However, the estimated NO_x lifetime of 3.7 hours seems to be too short in comparison with literature (Beirle et al., 2011; Beirle et al., 2004; Schaub et al., 2007).

This estimated NO_x lifetime by the column model is to a large extent determined by the decline in the line density downwind of the source area. Here four effects were tested that influence the downwind decay that were not yet incorporated in the column model: downwind emissions, a diurnal emission cycle, variability in lifetime and background decay. Downwind emissions that continuously add NO_2 caused a slower decline in the line density and hence a longer estimated lifetime. Accounting for this effect resulted in the longest lifetime from the four experiments: 3 times longer than the standard column model, resulting in a NO_x emission that is only 7.1% lower than the reference case. Hence it can be concluded that these four effects have large impacts on the estimated NO_x lifetime, but that their impact on the estimated NO_x emission is only minor. This can be explained by the fact that the emission is defined by the increase in line density over the city and that the emission is dominant compared to chemical decay. Yet it remains difficult to obtain an accurate estimate of the NO_x lifetime by fitting an exponential function through the downwind decay in the line density.

Because of this complexity in obtaining the NO_x lifetime from the downwind decay, the NO_x emission was estimated just from the accumulation over the city with a prescribed lifetime from a chemical reanalysis. This was done not only for 22 November 2017, but also for four days in February and six days in April 2018. Surface observations in Paris for these days showed a similar variation in magnitude in space as the TROPOMI observations, which confirms the increase of NO_2 in the wind direction in the line densities. The resulting averaged NO_x emission estimates are twice as strong during weekdays (55.9 mol s^{-1}) than during weekends (30.2 mol s^{-1}) and respectively 24% and 51% lower than the EDGAR emission inventory for Paris from 2012 with temporal correction. Although these lower values can partly be explained by the reported NO_x reduction since 2012, it should be noted that comparing these top-down estimates with the bottom-up inventory requires caution, as the uncertainty in the temporal correction factors seems to be large.

It is recommended to further improve this research by validating the TROPOMI observations, analysing the vertical distribution of NO_x over a source area such as Paris and how this relates to the wind speed, and replacing the average NO_x/NO_2 ratio with either simulated or measured values. But most importantly, extending this approach for more days and to other source areas could give better insights into the variation of the NO_x emission in time and around the world.

Once this method is applied more widely and further evaluated, it could become an understandable and fast addition to the existing bottom-up emission accounting and provide better insight into the magnitude, as well as the spatial and temporal variation of NO_x emissions. An important advantage is that this method is easy to understand: the TROPOMI observations give a good visualisation of how NO_x is added to the atmosphere from a large emission source. Yet

the strongest point of this approach is NO_x emissions can be quantified day-to-day, given that the source area is not covered by clouds and the wind speed is not very low. This allows to examine the seasonal and weekly emission cycle, from which the contribution of different emission sources can be deduced since emissions from residential heating take place during the winter and traffic emissions are strongest during weekdays. This can be an important tool for evaluating air quality and climate mitigation measures, not only for Paris' new atmospheric protection plan, but also for other large NO_x emissions sources all around the world.

References

Airparif, 2018: Air quality in the Paris region. [Available online at https://www.Airparif.asso.fr/_pdf/publications/bilan-2017-anglais20180829.pdf.]

Akimoto, H., T. Ohara, J. Kurokawa, and N. Horii, 2006: Verification of energy consumption in China during 1996-2003 by using satellite observational data. Atmos Environ, 40, 7663-7667.10.1016/j.atmosenv.2006.07.052

Beirle, S., K. F. Boersma, U. Platt, M. G. Lawrence, and T. Wagner, 2011: Megacity Emissions and Lifetimes of Nitrogen Oxides Probed from Space. Science, 333, 1737-1739.10.1126/science.1207824

Beirle, S., U. Platt, R. von Glasow, M. Wenig, and T. Wagner, 2004: Estimate of nitrogen oxide emissions from shipping by satellite remote sensing. Geophys Res Lett, 31.Artn L18102 10.1029/2004gl020312

Beirle, S., U. Platt, M. Wenig, and T. Wagner, 2003: Weekly cycle of NO2 by GOME measurements: a signature of anthropogenic sources. Atmos Chem Phys, 3, 2225-2232.DOI 10.5194/acp-3-2225-2003

Boersma, K. F., and Coauthors, 2011: An improved tropospheric NO2 column retrieval algorithm for the Ozone Monitoring Instrument. Atmos Meas Tech, 4, 1905-1928.10.5194/amt-4-1905-2011

Boersma, K. F., and Coauthors, 2018: Improving algorithms and uncertainty estimates for satellite NO2 retrievals: Results from the Quality Assurance for Essential Climate Variables (QA4ECV) project. Atmos. Meas. Tech. Discuss., 2018, 1-70.10.5194/amt-2018-200

Boersma, K. F., D. J. Jacob, H. J. Eskes, R. W. Pinder, J. Wang, and R. J. van der A, 2008: Intercomparison of SCIAMACHY and OMI tropospheric NO2 columns: Observing the diurnal evolution of chemistry and emissions from space. Journal of Geophysical Research: Atmospheres, 113.doi:10.1029/2007JD008816

Boersma, K. F., and Coauthors, 2016: Product Specification Document for the QA4ECV NO2 ECV precursor product

Bucsela, E. J., and Coauthors, 2013: A new stratospheric and tropospheric NO2 retrieval algorithm for nadir-viewing satellite instruments: applications to OMI. Atmos Meas Tech, 6, 2607-2626.10.5194/amt-6-2607-2013

Butler, T. M., M. G. Lawrence, B. R. Gurjar, J. Van Aardenne, M. Schultz, and J. Lelieveld, 2008: The representation of emissions from megacities in global emission inventories. Atmos Environ, 42, 703-719.10.1016/j.atmosenv.2007.09.060

Crippa, M., and Coauthors, 2018: Gridded emissions of air pollutants for the period 1970–2012 within EDGAR v4. 3.2. Earth System Science Data, 10, 1987-2013,

Crippa, M., and Coauthors, 2016: Forty years of improvements in European air quality: regional policy-industry interactions with global impacts. Atmos. Chem. Phys., 16, 3825-3841.10.5194/acp-16-3825-2016

de Foy, B., J. L. Wilkins, Z. Lu, D. G. Streets, and B. N. Duncan, 2014: Model evaluation of methods for estimating surface emissions and chemical lifetimes from satellite data. Atmos Environ, 98, 66-77,

Dieudonné, E., F. Ravetta, J. Pelon, F. Goutail, and J.-P. Pommereau, 2013: Linking NO2 surface concentration and integrated content in the urban developed atmospheric boundary layer. Geophys Res Lett, 40, 1247-1251.doi:10.1002/grl.50242

Direction Regionale et Interdepartementale de l'Environnement et de l'Energie [DRIEE], 2018: Plan de Protection de l'Atmosphere d'Ile-de-France. [Available online at https://www.maqualitedelair-idf.fr/w2020/wp-content/uploads/2018/02/PPAjanvier18-sans-fiche.pdf.]

European Environmental Agency [EEA], 2017: National emissions reported to the Convention on Long-range Transboundary Air Pollution (LRTAP Convention). [Available online at https://www.eea.europa.eu/data-and-maps/data/national-emissions-reported-to-the-convention-on-long-range-transboundary-air-pollution-lrtap-convention-12tab-european-data.]

European Environmental Agency [EEA], E. E. A., 2013: Emission Inventory guidebook. [Available online at https://www.eea.europa. eu/publications/emep-eea-guidebook-2013.]

G., J.-M., and Coauthors, 2017: EDGAR v4.3.2 Global Atlas of the three major Greenhouse Gas Emissions for the period 1970-2012. Earth System Science Data Discussions.https://doi.org/10.5194/essd-2017-79

Jacob, D. J., 1999: Introduction to atmospheric chemistry. Princeton University Press, xii, 266 p. pp.

Janssens-Maenhout, G., and Coauthors, 2015: HTAP_v2. 2: a mosaic of regional and global emission grid maps for 2008 and 2010 to study hemispheric transport of air pollution. Atmos Chem Phys, 15, 11411-11432,

Jiang, Z., and Coauthors, 2018: Unexpected slowdown of US pollutant emission reduction in the past decade. Proceedings of the National Academy of Sciences, 115, 5099-5104.10.1073/pnas.1801191115

Kanaya, Y., and Coauthors, 2007: Urban photochemistry in central Tokyo: 1. Observed and modeled OH and HO2 radical concentrations during the winter and summer of 2004. Journal of Geophysical Research: Atmospheres, 112,

Krijger, J. M., M. van Weele, I. Aben, and R. Frey, 2007: Technical Note: The effect of sensor resolution on the number of cloud-free observations from space. Atmos. Chem. Phys., 7, 2881-2891.10.5194/acp-7-2881-

Kuenen, J. J. P., A. J. H. Visschedijk, M. Jozwicka, and H. A. C. D. van der Gon, 2014: TNO-MACC_II emission inventory; a multi-year (2003-2009) consistent high-resolution European emission inventory for air quality modelling. Atmos Chem Phys, 14, 10963-10976.10.5194/acp-14-10963-2014

Lin, J. T., M. B. McElroy, and K. F. Boersma, 2010: Constraint of anthropogenic NOx emissions in China from different sectors: a new methodology using multiple satellite retrievals. Atmos Chem Phys, 10, 63-78.DOI 10.5194/acp-10-63-2010,

Lorente, A., and Coauthors, 2018: Quantification of nitrogen oxides emissions from build-up of pollution over Paris with S5P-TROPOMI. Unpublished manuscript.,

Martin, R. V., D. J. Jacob, K. Chance, T. P. Kurosu, P. I. Palmer, and M. J. Evans, 2003: Global inventory of nitrogen oxide emissions constrained by space-based observations of NO2 columns. J Geophys Res-Atmos, 108.Artn 4537. 10.1029/2003jd003453,

Michoud, V., and Coauthors, 2012: Radical budget analysis in a suburban European site during the MEGAPOLI summer field campaign. Atmos Chem Phys, 12, 11951-11974,

Richter, A., J. P. Burrows, H. Nuss, C. Granier, and U. Niemeier, 2005: Increase in tropospheric nitrogen dioxide over China observed from space. Nature, 437, 129-132.10.1038/nature04092

Schaub, D., and Coauthors, 2007: SCIAMACHY tropospheric NO 2 over Switzerland: estimates of NO x lifetimes and impact of the complex Alpine topography on the retrieval. Atmos Chem Phys, 7, 5971-5987,

Seinfeld, J. H., and S. N. Pandis, 2012: Atmospheric chemistry and physics: from air pollution to climate change. John Wiley Sons.

Shaiganfar, R., and Coauthors, 2017: Estimation of the Paris NO x emissions from mobile MAX-DOAS observations and CHIMERE model simulations during the MEGAPOLI campaign using

the closed integral method. Atmos Chem Phys, 17, 7853,

van der Gon, H. A. C. D., C. Hendriks, J. J. P. Kuenen, A. Segers, and A. J. H. Visschedijk, 2011: Description of current temporal emission patterns and sensitivity of predicted AQ for temporal emission patterns

van Geffen, J., K. F. Boersma, H. J. Eskes, J. D. Maasakkers, and J. P. Veefkind, 2016: TROPOMI ATBD of the total and tropospheric NO2 data productsS5P-KNMI-L2-0005-RP

Veefkind, J. P., and Coauthors, 2012: TROPOMI on the ESA Sentinel-5 Precursor: A GMES mission for global observations of the atmospheric composition for climate, air quality and ozone layer applications. Remote Sens Environ, 120, 70-83.10.1016/j.rse.2011.09.027

Vinken, G. C. M., K. F. Boersma, A. van Donkelaar, and L. Zhang, 2014: Constraints on ship NOx emissions in Europe using GEOS-Chem and OMI satellite NO2 observations. Atmos Chem Phys, 14, 1353-1369.10.5194/acp-14-1353-2014

Wang, S. W., and Coauthors, 2012: Growth in NOx emissions from power plants in China: bottom-up estimates and satellite observations. Atmos Chem Phys, 12, 4429-4447.10.5194/acp-12-4429-2012

World Health Organization [WHO], W. H. O., cited 2018: Ambient (outdoor) air quality and health. [Available online at http://www.who.int/mediacentre/factsheets/fs313/en/.]